ARMY RESEARCH LABORATORY

Battlescale Forecast Model and its Evaluation Using White Sands Missile Range Meteorological Data

by Teizi Henmi
M. E. Lee
Battlefield Environment Directorate
and
T. J. Smith
Operating Location N, Air Weather Service

ARL-TR-569 April 1995

NOTICES

Disclaimers

The findings in this report are not to be construed as an official Department of the Army position, unless so designated by other authorized documents.

The citation of trade names and names of manufacturers in this report is not to be construed as official Government indorse-ment or approval of commercial products or services referenced herein.

Destruction Notice

When this document is no longer needed, destroy it by any method that will prevent disclosure of its contents or reconstruction of the document.

REPORT DOCUMENTATION PAGE

Form Approved
OMB No. 0704-0188

1. AGENCY USE ONLY *(Leave blank)*	2. REPORT DATE	3. REPORT TYPE AND DATES COVERED
	April 1995	Final

4. TITLE AND SUBTITLE

Battlescale Forecast Model and its Evaluation Using White Sands Missile Range Meteorological Data

5. FUNDING NUMBERS

6. AUTHOR(S)

Teizi Henmi, M. E. Lee, (BED)
and T. J. Smith (Operating Location N, Air Weather Service)

7. PERFORMING ORGANIZATION NAME(S) AND ADDRESS(ES)

U.S. Army Research Laboratory
Battlefield Environment Directorate
ATTN: AMSRL-BED
White Sands Missile Range, NM 88002-5501

8. PERFORMING ORGANIZATION REPORT NUMBER

ARL-TR-569

9. SPONSORING / MONITORING AGENCY NAME(S) AND ADDRESS(ES)

U.S. Army Research Laboratory
2800 Powder Mill Road
Adelphi, MD 20783-1145

10. SPONSORING / MONITORING AGENCY REPORT NUMBER

ARL-TR-569

11. SUPPLEMENTARY NOTES

12a. DISTRIBUTION / AVAILABILITY STATEMENT

Approved for public release; distribution is unlimited.

12b. DISTRIBUTION CODE

A

13. ABSTRACT *(Maximum 200 words)*

The Battlescale Forecast Model (BFM) was developed by the U.S. Army Research Laboratory for operational short-range (12-h) forecast. The BFM is composed of two major programs. The first program, called 3dobj, creates initial and boundary values for a forecast model by analyzing the U.S. Air Force Global Spectral Model (GSM) forecast field output data and upper air sounding data if it is available. The second program is a forecast model adapted from the Higher Order Turbulence Model for Atmospheric Circulation developed by Yamada.*

From a case study of wind field variation, it became clear that wind fields interpolated from GSM data deviated significantly from those observed because of coarse grid spacing and lack of boundary layer physics of the GSM. Thus, it is concluded that incorporation of observed surface wind data into the initial field is important.

The performance of the BFM is evaluated using meteorological data observed at White Sands Missile Range, NM. Three different initialization methods are examined to identify optimal model initialization methods. Statistical parameters such as mean residual fields of surface wind and temperature are derived from comparisons of corresponding observations and 25 12-h forecast calculations. Results indicate that incorporation of surface wind observation data into the initial field is essential to produce good, short-range BFM forecasts.

*Yamada T. and S. Bunker, "A Numerical Study of Nocturnal Drainage Flows with Stong Wind and Temperature Gradients," *J. Appl. Metero.*, **28**, p 545-554, 1989.

14. SUBJECT TERMS	15. NUMBER OF PAGES
battlescale, mesoscale, evaluation	82
	16. PRICE CODE

17. SECURITY CLASSIFICATION OF REPORT	18. SECURITY CLASSIFICATION OF THIS PAGE	19. SECURITY CLASSIFICATION OF ABSTRACT	20. LIMITATION OF ABSTRACT
Unclassified	Unclassified	Unclassified	SAR

Contents

Figures

Table

1. Introduction

The U.S. Army Research Laboratory (ARL) has developed the Battlescale Forecast Model (BFM) for operational short-range (12-h) forecasting over an area of 500 by 500 km or smaller. The BFM will become a major part of the Integrated Meteorological System Block 2 software.

The BFM is composed of two major programs. The first part of the program, called 3dobj, creates initial and boundary values for a forecast model by analyzing the U.S. Air Force Global Spectral Model (GSM) forecast field output data and upper air sounding data if it is available. In the second part of the program, a forecast model was adapted from a mesoscale meteorological model called the Higher Order Turbulence Model for Atmospheric Circulation (HOTMAC) developed by Yamada. [1] HOTMAC has been used extensively at ARL [2,3,4] and can simulate the evolution of locally forced circulations due to surface heating and cooling over meso-β and γ scale areas. HOTMAC is numerically stable and easy to use; therefore, it is suitable for operational use.

In the present study, the forecasting capability of the BFM is evaluated by comparing the model computed results with surface and upper air data obtained by the Surface Automated Meteorological System (SAMS) and the Atmospheric Profiler Research Facility (APRF), respectively, located at the White Sands Missile Range (WSMR), NM. The APRF operates 49.25-, 404.37-, and 924-MHz profilers and a monostatic acoustic sounder and provides vertical profiles of wind and temperature. In a case study described in this report, 12-h forecastings for the period from 05 to 17 local standard time (LST) of 10 Mar 94 were made using different initialization methods. On this day, surface wind direction over WSMR varied from north in the early morning to south in the late morning. To simulate this wind direction shift, three different initialization methods were examined.

The three methods were applied to 25 12-h forecast periods, and the forecast results of surface wind components and temperature were compared with SAMS observational data. In addition, temporal and spatial linear interpolation of the GSM grid values was done, and the values were compared with observation.

Additionally, horizontal components of surface winds at the SAMS sites were assimilated by nudging every 3 h into the model calculation and compared with the observation. The comparison results of three initialization methods and two additional methods were evaluated using statistical parameters such as mean residuals and standard deviation of mean residuals.

The purposes of this report are to describe the BFM, the results of the case study, and statistical evaluation of forecast results.

2. BFM

2.1 HOTMAC

The basic equations for HOTMAC are the conservation equations for mass, momentum, potential temperature, mixing ratio of water vapor, and turbulence kinetic energy. [5]

The potential temperature equation was modified so the deviation of potential temperature of the large-scale flow at an initial state was solved. [1] The modification was to maintain stable numerical simulations and realistically-predicted wind fields when HOTMAC was applied to simulate air flows over complex terrain with strong wind shear and temperature inversion. [5] The large-scale temperature was allowed to vary with space.

Also referred to as a second-moment turbulence-closure model, HOTMAC is based on a set of second-moment turbulence equations closed by assuming certain relationships between unknown higher-order turbulence moments and the known lower-order moments. HOTMAC can be used under general conditions of flow and thermal stratification; methods for turbulence parameterization are more advanced than those in simple eddy viscosity models. The present model, referred to as the Level 2.5 model, [6] solves a prognostic equation for turbulence kinetic energy only; the remaining second-moment turbulence variables, such as standard deviations of wind components and heat and momentum fluxes, are solved from a set of algebraic equations.

The present model assumes hydrostatic equilibrium and uses the Boussinesq approximation. Therefore, in theory, the model applications are limited to flows where the local acceleration and advection terms in the equation of vertical motion are much smaller than the acceleration caused by gravity (hydrostatic equilibrium) and temperature variations in the horizontal directions are not too large (Boussinesq approximation). This assumption is probably satisfied with a horizontal grid spacing greater than a few kilometers. The only way to assure that these assumptions are reasonable is to repeat the simulations with a nonhydrostatic, non-Boussinesq mesoscale model, and compare the

results with the present results. It is very complicated and almost impossible to construct a non-Boussinesq turbulence closure model.

Surface boundary conditions were constructed from the empirical formulas of Dyer and Hicks [7] for nondimensional wind and temperature profiles. The temperatures in the soil layers were obtained by solutions of the heat conduction equation. Appropriate boundary conditions were the heat balance at the soil surface and specification of the soil temperature at a certain depth. The lateral boundary values of horizontal wind components, potential temperature, moisture mixing ratio, and turbulence kinetic energy were obtained by integration of the corresponding governing equations, except variations in the horizontal directions were neglected. Parameterization of tall canopy effects on wind and radiation has been studied; [8] the effects are included in the present model.

The governing equations were integrated by use of the Alternating Direction Implicit method. [9] A time increment was chosen to be 90 percent of the minimum value of $\Delta x_i/U_i$, where Δx_i is a grid spacing and U_i the velocity component in the i-th direction (Courant-Freidrich-Lewy criterion). The integration time increment is also limited by the propagation speed of gravity waves computed based on the potential temperature gradients. To increase the accuracy of finite-difference approximations, mean and turbulence variables are defined at grids staggered in the horizontal and vertical directions. Mean winds, temperature, and water vapor vary most with height near the surface. To resolve the variations without introducing an excessive computational burden, nonuniform grid spacing is used in the vertical direction.

To assimilate observed data into the model calculation, nudging terms were added to the model equations. Assimilations of data by nudging are made to initialize the forecast calculation and provide time-dependent lateral boundary values.

2.2 Nudging Method

By adding nudging terms, the equations of horizontal wind components are modified as follows:

$$\frac{\partial U}{\partial t} = F_1 + C_n(U_t - U) \tag{1}$$

$$\frac{\partial V}{\partial t} = F_2 + C_n(V_t - V) \tag{2}$$

where

U_t = the target wind component of the x direction
V_t = the target wind component of the y direction.

U_t and V_t are described in the following section.

The equations of potential temperature deviation and mixing ratio are written with nudging terms as follows:

$$\frac{\partial \delta\theta}{\partial t} = F_3 + C_n(\delta\theta_{obs} - \delta\theta) \tag{3}$$

$$\frac{\partial q}{\partial t} = F_4 + C_n(q_{obs} - q) \tag{4}$$

where

C_n = the nudging coefficient (a constant value of 5×10^{-4} is employed)
$\delta\theta$ = the deviation of potential temperature from an initial potential temperature
q = water vapor mixing ratio.

F_1, F_2, F_3, and F_4 are the terms found in HOTMAC equations. [1]

2.3 Target Wind

Comparisons in the simulated wind fields, found by nudging to the target wind components U_t and V_t and by nudging to the observed wind components U_{obs} and V_{obs}, were conducted. [10] It was shown that nudging to the target wind components produces better agreement between simulated and observed upper winds than nudging to the observed wind components.

Target wind components U_t and V_t are derived as follows. The equations of motion with the target wind under no frictional force can be written as follows:

$$\frac{\partial U}{\partial t} = f\,(V - V_g) + C_n(U_t - U) \tag{5}$$

$$\frac{\partial V}{\partial t} = -f\,(U - U_g) + C_n(V_t - V). \tag{6}$$

The solutions to the above equations at equilibrium are given by the following:

$$U = \frac{f\,C_n(V_t - V_g) + f^2 U_g + C_n^2 U_t}{C_n^2 + f^2} \tag{7}$$

$$V = \frac{-f\,C_n(U_t - U_g) + f^2 V_g + C_n^2 V_t}{C_n^2 + f^2}. \tag{8}$$

Letting U and V approach U_{obs} and V_{obs}, respectively, and solving for U_t and V_t, the following equations are obtained:

$$U_t = U_{obs} - \frac{f}{C_n}(V_{obs} - V_g) \tag{9}$$

$$V_t = V_{obs} + \frac{f}{C_n}(U_{obs} - U_g) \tag{10}$$

where

U_{obs} and V_{obs} = the observed wind components

U_g and V_g = the geostrophic wind components.

The formulas for U_g and V_g can be found in Yamada [11] and Yamada and Bunker. [1] U_t and V_t are, in general, different from the corresponding large-scale wind components. Observed winds may be used as target winds if the Coriolis force is absent or if the observed winds are identical to the geostrophic winds. If only the observed winds are used in the nudging in all other cases, the solutions will generally be different from the observations.

The physical meaning of the target winds is that the solutions of the equations of motions with the target winds become identical to the observed winds in the absence of frictional effects. Thus, modeled winds should converge to observations in the layers far above the boundary layer where frictional effects are negligible. On the other hand, atmospheric turbulence in the boundary layer is significant because of frictional effects, and the nudging terms play relatively minor roles. In summary, the nudging terms enforce the modeled winds to match observations in the free atmosphere, but they play relatively minor roles in the boundary layer.

3. Model Domain and Observed Data

The study area was centered over WSMR, NM. Figure 1 shows terrain elevation distribution in the area covering 800 by 800 km. The latitude and longitude of the center of the area are, 33.20 N and 106.41 W, respectively. The area within the inner square covers 250 by 250 km, and forecast computation was conducted over this area. Meteorological variables are calculated at 51 by 51 by 16 grid points with unit horizontal grid distance of 5 km. The top-of-the-model atmosphere is 7000 m above the highest elevation in the domain.

GSM output is reported on grid points spaced 381 km apart on the mandatory pressure surfaces, as marked by an asterisk in figure 1. Three-dimensional (3-D) objective analyses of GSM data were made over the area covering 800 by 800 km, and the data over 250 by 250 km were used for forecast computation. Figure 2 shows detailed elevation distribution of the forecast computation domain. The locations of SAMS at WSMR are marked by Arabic numbers.

For this study, 12-h forecasting computations were made for 25 periods during Feb and Mar 94, as shown in table 1.

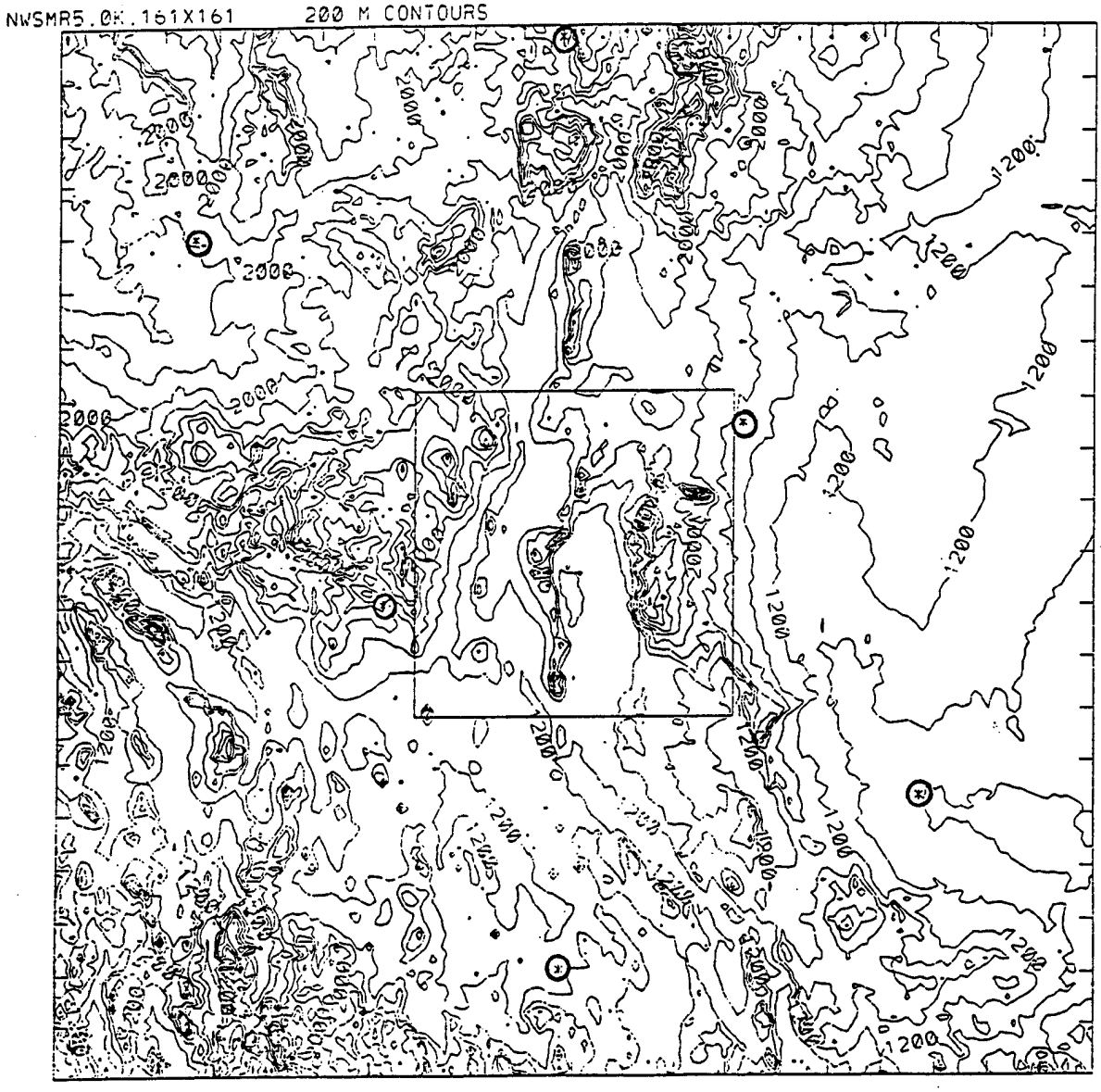

Figure 1. Elevation data with 200-m contours containing an 800- by 800-km area of the Southwestern United States. The longitude and latitude of the center are 106.406 W and 33.200 N. The locations of GSM grid points are marked by *. The area surrounded by a square is the domain of the BFM for the present study (200 by 200 km).

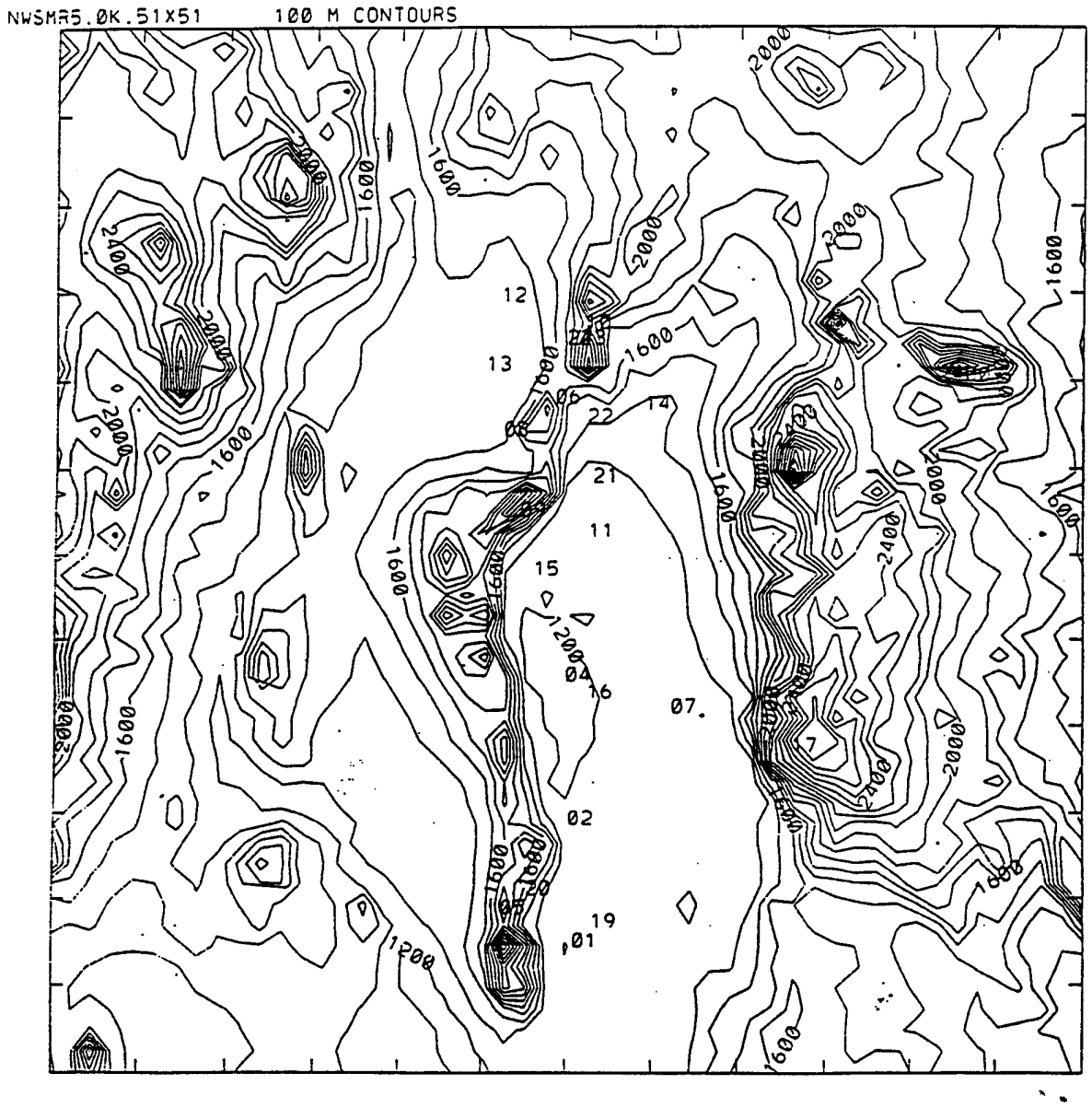

Figure 2. Domain of the BFM for the present study covering the area of 250 by 250 km. Contour lines are drawn every 200 m. The locations of SAMS are marked by numbers.

Table 1. Twenty five 12-h periods during Feb and Mar 94, used for forecast calculations in the present study

Forecast Period		
Period	Date	Period (GMT)
1	2 Feb	12 - 00
2	3 Feb	00 - 12
3	17 Feb	00 - 12
4	17 Feb	12 - 00
5	18 Feb	00 - 12
6	18 Feb	12 - 00
7	23 Feb	00 - 12
8	23 Feb	12 - 00
9	24 Feb	12 - 00
10	24 Feb	12 - 00
11	2 Mar	12 - 00
12	2 Mar	12 - 00
13	3 Mar	00 - 12
14	3 Mar	12 - 00
15	4 Mar	00 - 12
16	7 Mar	00 - 12
17	7 Mar	12 - 00
18	8 Mar	00 - 12
19	9 Mar	00 - 12
20	9 Mar	12 - 00
21	10 Mar	00 - 12
22	10 Mar	12 - 00
23	15 Mar	00 - 12
24	16 Mar	00 - 12
25	16 Mar	12 - 00

4. Case Study Overview

A major reason the initialization methods in sections 5.2 and 5.3 are employed is based on the study of surface wind variation during the 12 h-period of 05 through 17 LST of 10 Mar 94 described in this section.

Figures 3 through 8 are observed surface wind vectors during the 12-h period from 05 to 17 LST on 10 Mar 94. During the morning hours until 10 LST, the prevailing wind directions in WSMR were predominantly from the north. Figure 5 shows that wind directions were transitioning to the southerly. At 12 LST, all the SAMS stations recorded southerly winds, and southerly winds were dominant in the afternoon.

Figures 9 and 10 show that the wind directions calculated from the GSM data were predominantly southerly at 05 and 17 LST, contrary to the observed surface wind variations. It is concluded that, to obtain good forecast of wind, incorporation of observed data into the initial wind vector field is necessary. A uniform wind vector field shown in figure 11 was the initial field at $z^* = 10$ m level calculated as the mean of the observed data at 05 LST on 10 Mar 94 and corresponds to the initialization time of forecast calculation.

Figures 12 through 15 are forecast surface wind fields based on the initial wind field shown in figure 11. Northerly or downslope winds are the main features until 10 LST in the morning. However, wind directions changed to southerly or upslope between 10 and 11 LST, and southerly or upslope components of wind are intensified during the afternoon. The transition of wind directions from northerly to southerly also occurred in the observed wind data (figures 3 through 8).

Figures 16 through 19 are also forecast surface wind fields corresponding to figures 12 through 15, except the forecast computation is initialized by the GSM data shown in figure 9. It is shown that the forecast computation initialized by the GSM failed to produce northerly wind vector distributions in the morning hours (figures 16 and 17). However, the afternoon wind fields become similar in the two cases (figures 14, 15, 18, and 19).

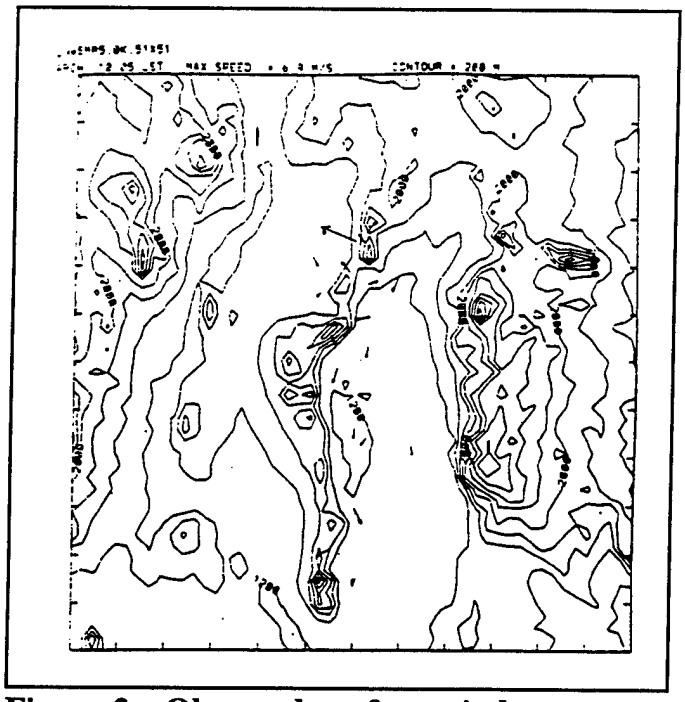

Figure 3. Observed surface wind vectors at WSMR on 10 Mar 94 at 05 LST, maximum vector is 6.9 m/s.

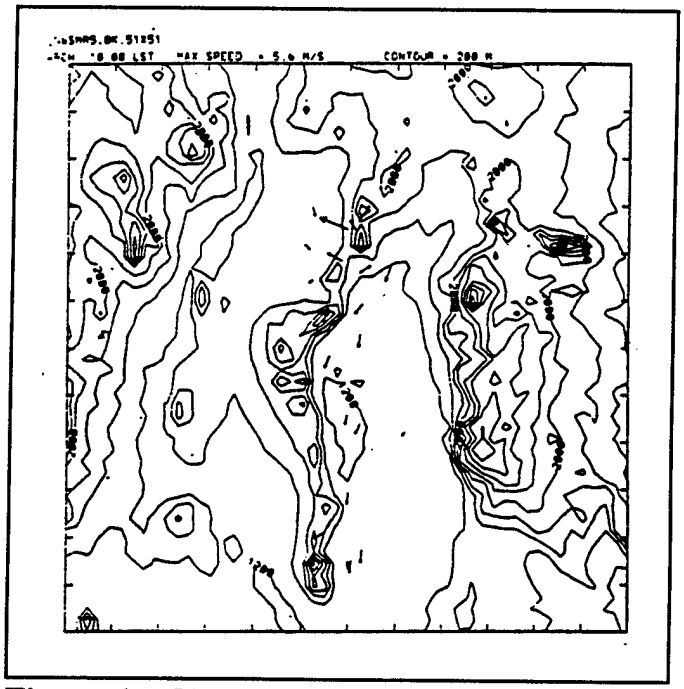

Figure 4. Observed surface wind vectors at WSMR on 10 Mar 94 at 08 LST, maximum vector is 5.6 m/s.

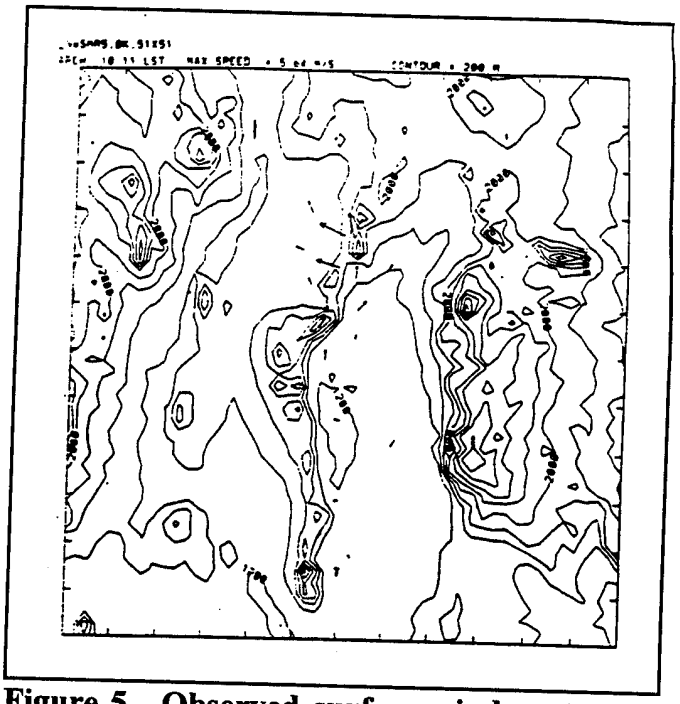

Figure 5. Observed surface wind vectors at WSMR on 10 Mar 94 at 11 LST, maximum vector is 5.64 m/s.

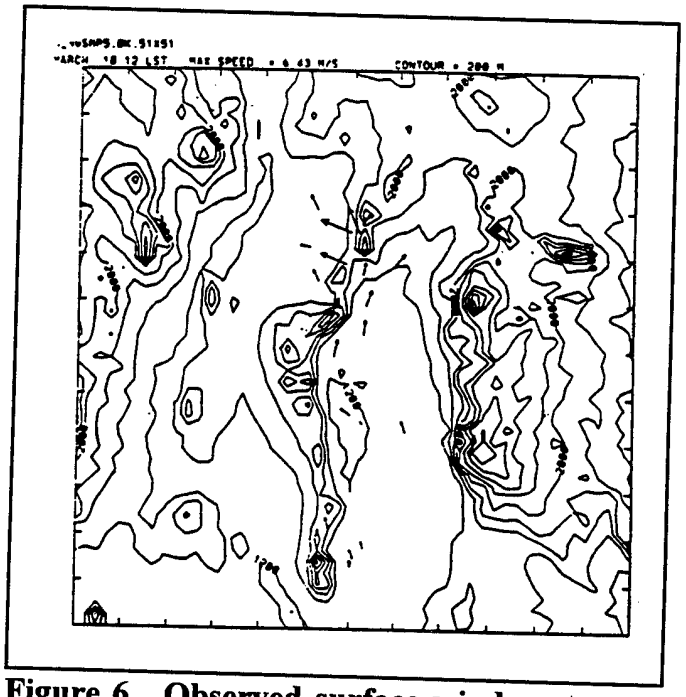

Figure 6. Observed surface wind vectors at WSMR on 10 Mar 94 at 12 LST, maximum vector 6.43 m/s.

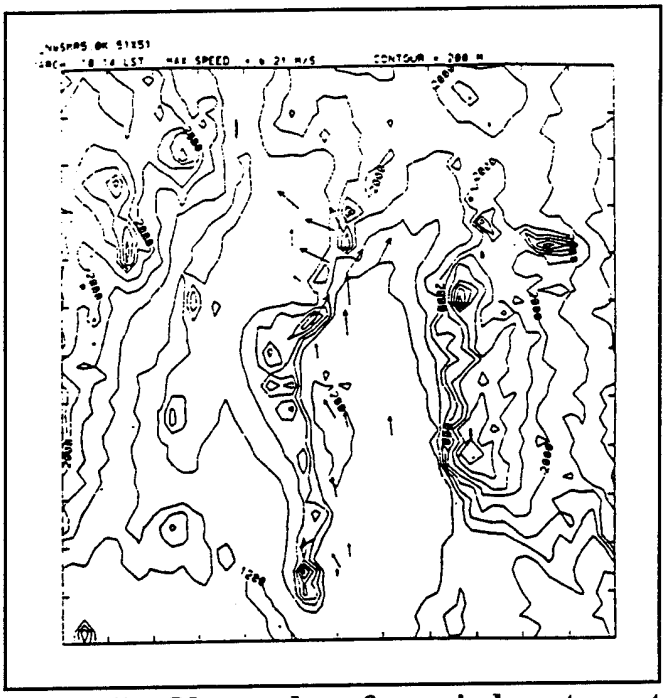

Figure 7. Observed surface wind vectors at WSMR on 10 Mar 94 at 14 LST, maximum vector 6.21 m/s.

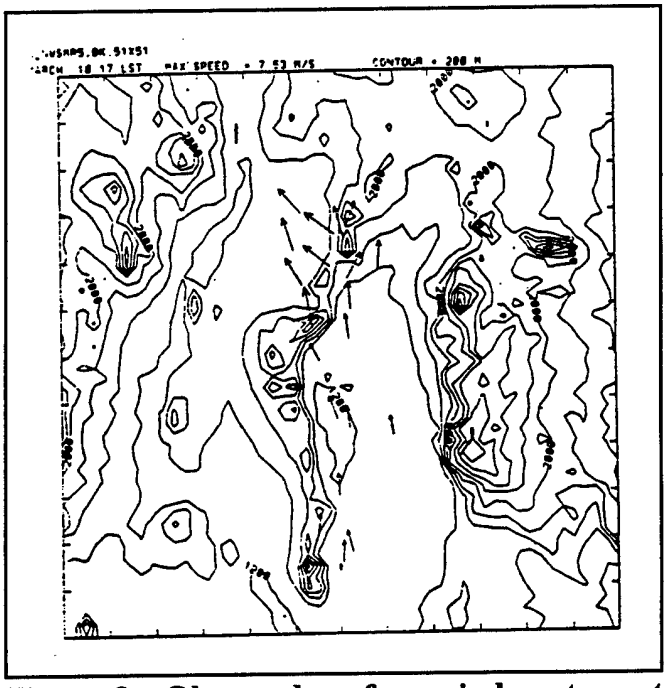

Figure 8. Observed surface wind vectors at WSMR on 10 Mar 94 at 17 LST, maximum vector 7.53 m/s.

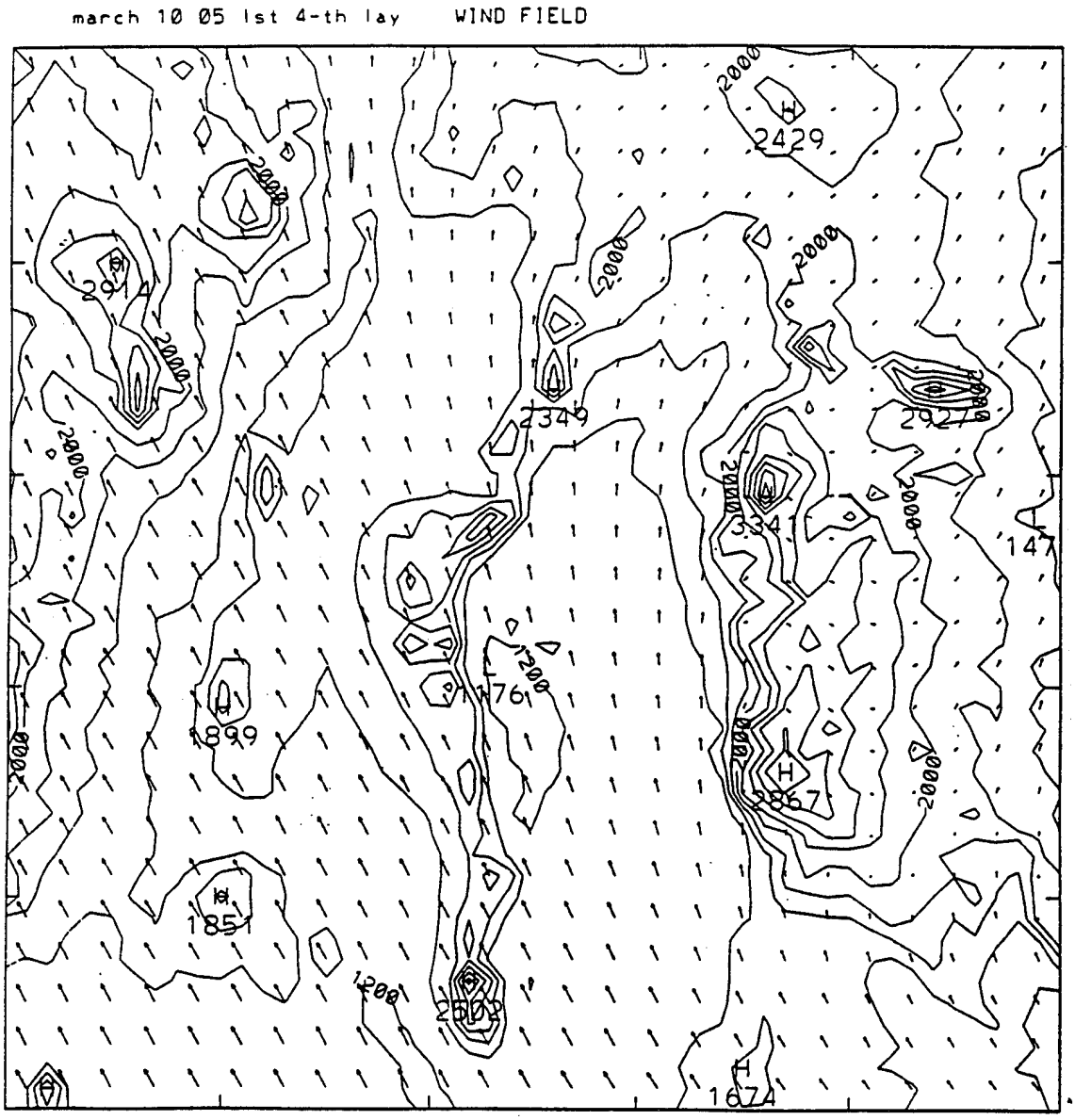

Figure 9. Surface wind vector distribution obtained from the analysis of GSM data at 05 LST on 10 Mar 94, maximum vector 10 m/s.

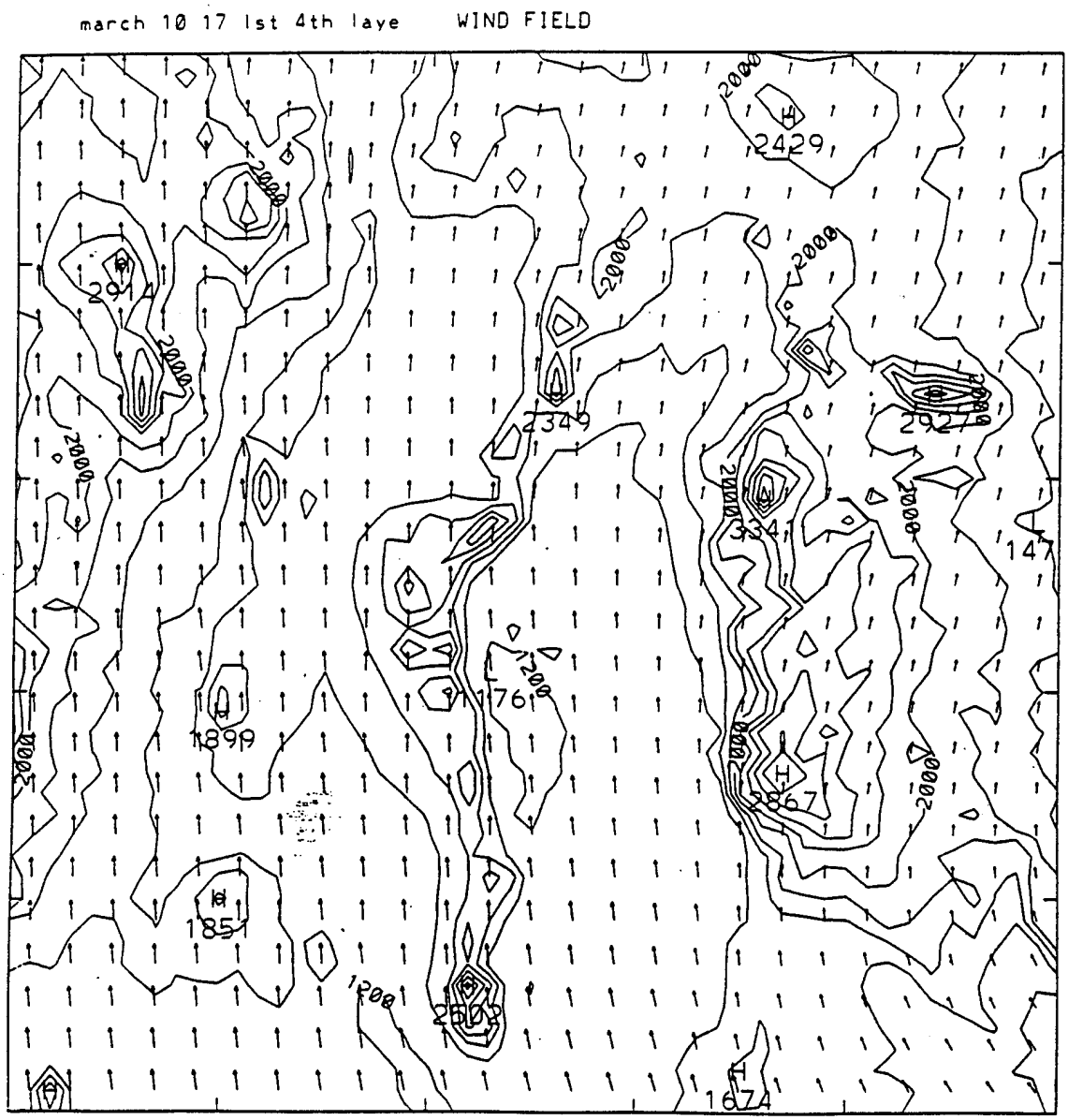

Figure 10. Surface wind vector distribution obtained from the analysis of GSM data at 17 LST on 10 Mar 94, maximum vector 12.7 m/s.

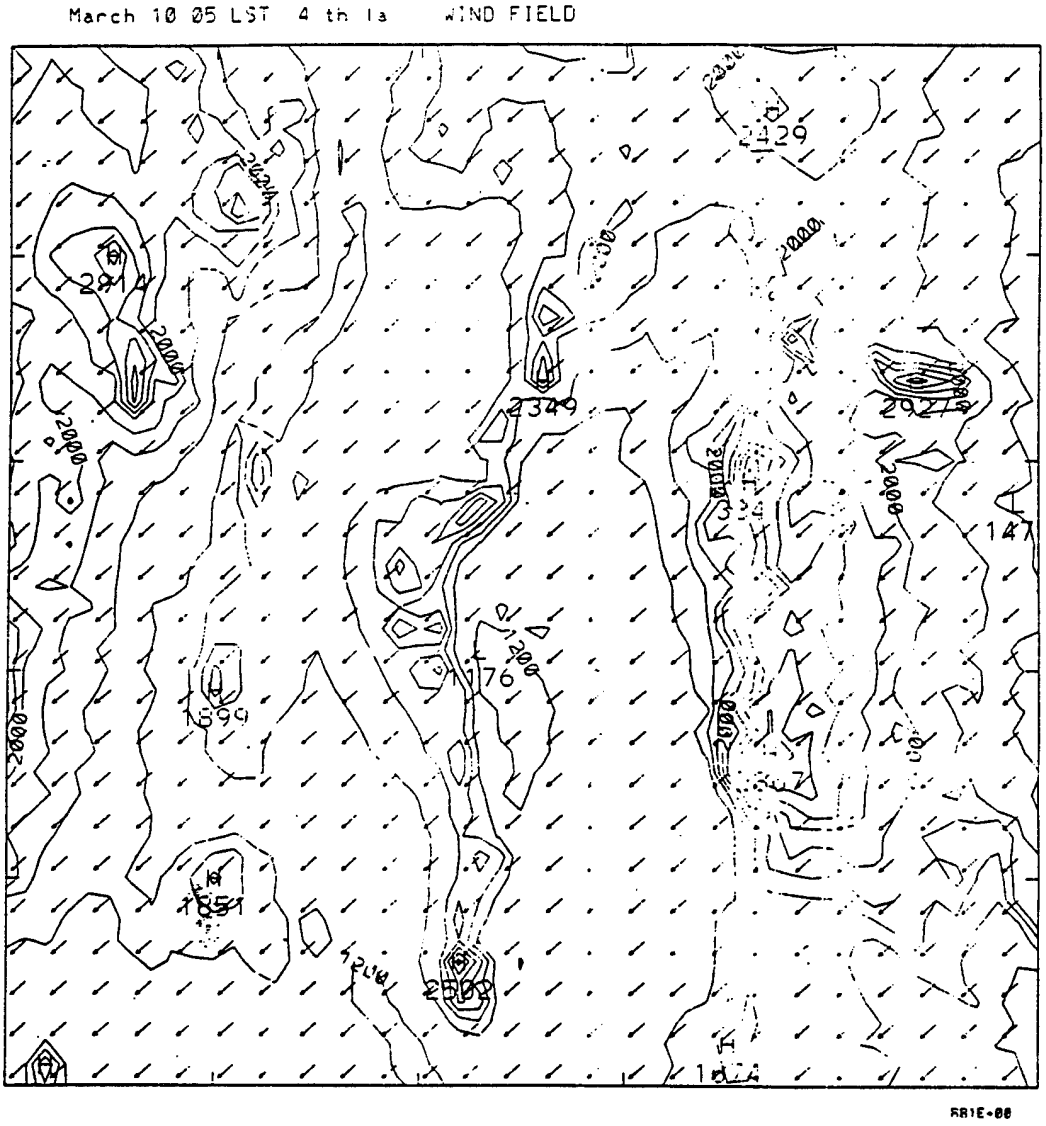

Figure 11. Wind vector field at z* = 10 m level, calculated from observed data at 05 LST on 10 Mar 94, maximum vector 8.81 m/s.

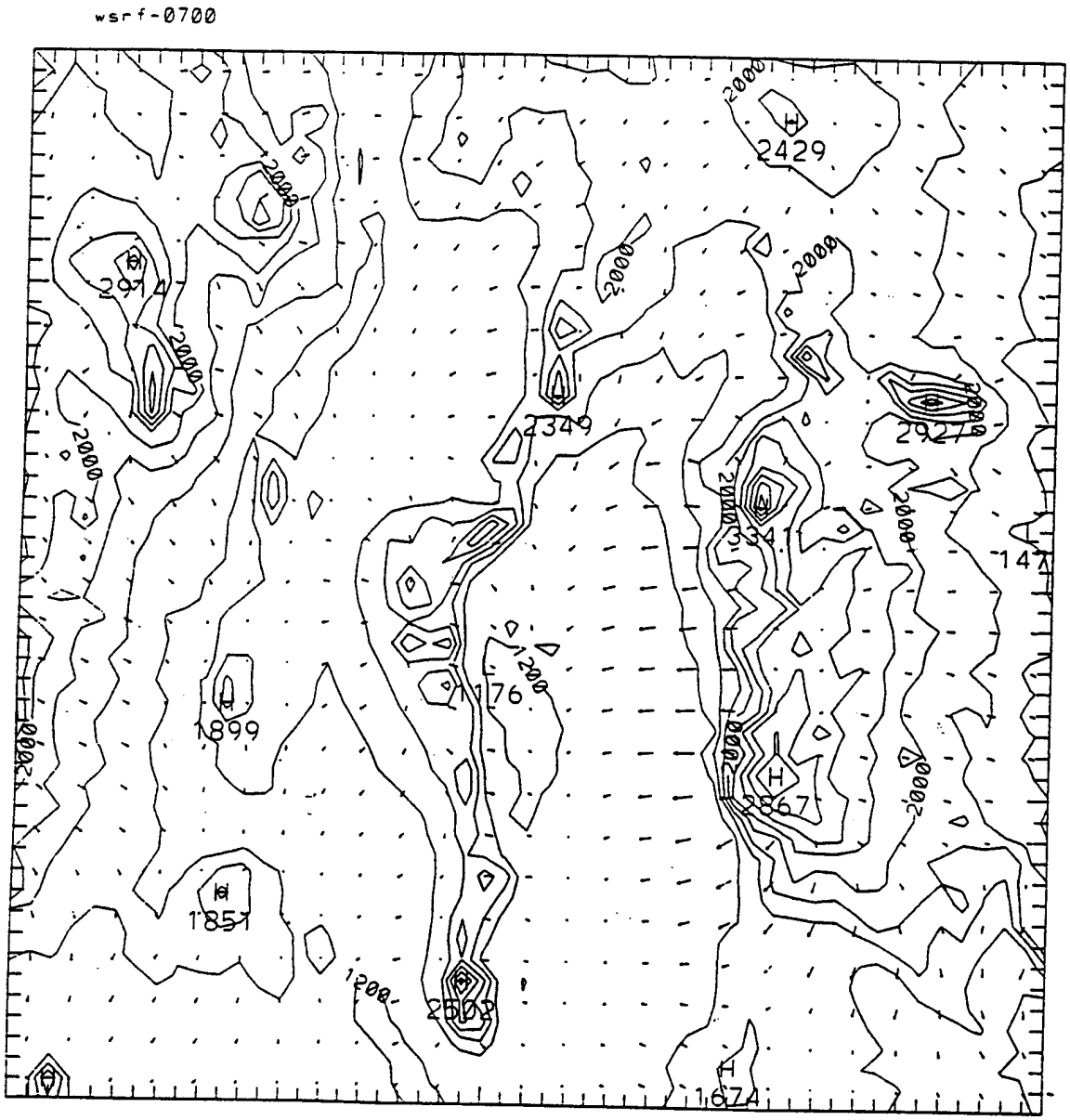

Figure 12. Forecast surface wind field at 7 LST on 10 Mar 94, maximum wind speed is 9.24 m/s. Initial wind field at 5 LST was calculated using mean speed and direction of SAMS stations.

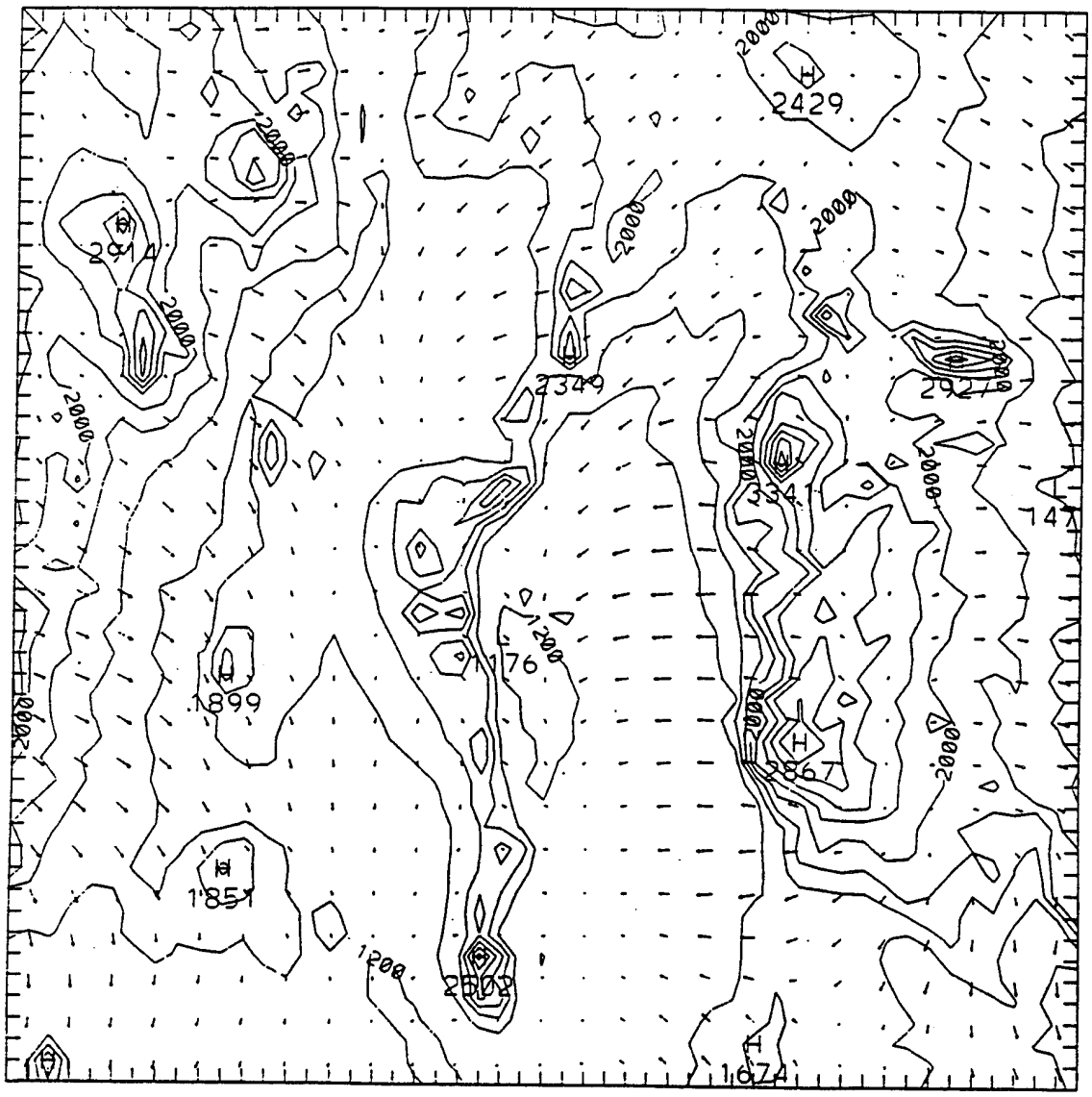

Figure 13. Forecast surface wind field at 10 LST on 10 Mar 94, maximum wind speed is 3.59 m/s. Initial wind field at 5 LST was calculated using mean speed and direction of SAMS stations.

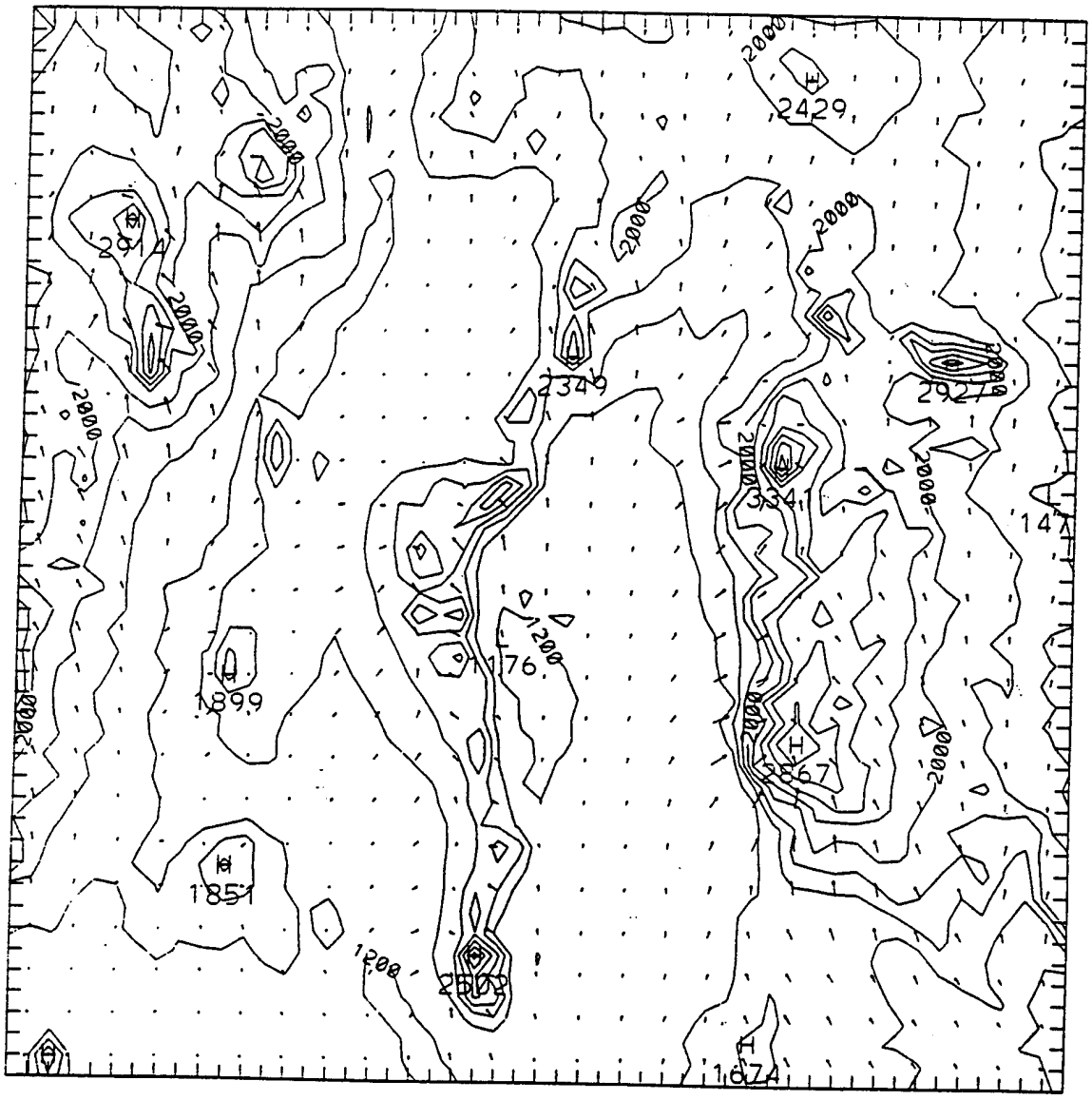

Figure 14. Forecast surface wind field at 11 LST on 10 Mar 94, maximum wind speed is 4.71 m/s. Initial wind field at 5 LST was calculated using mean speed and direction of SAMS stations.

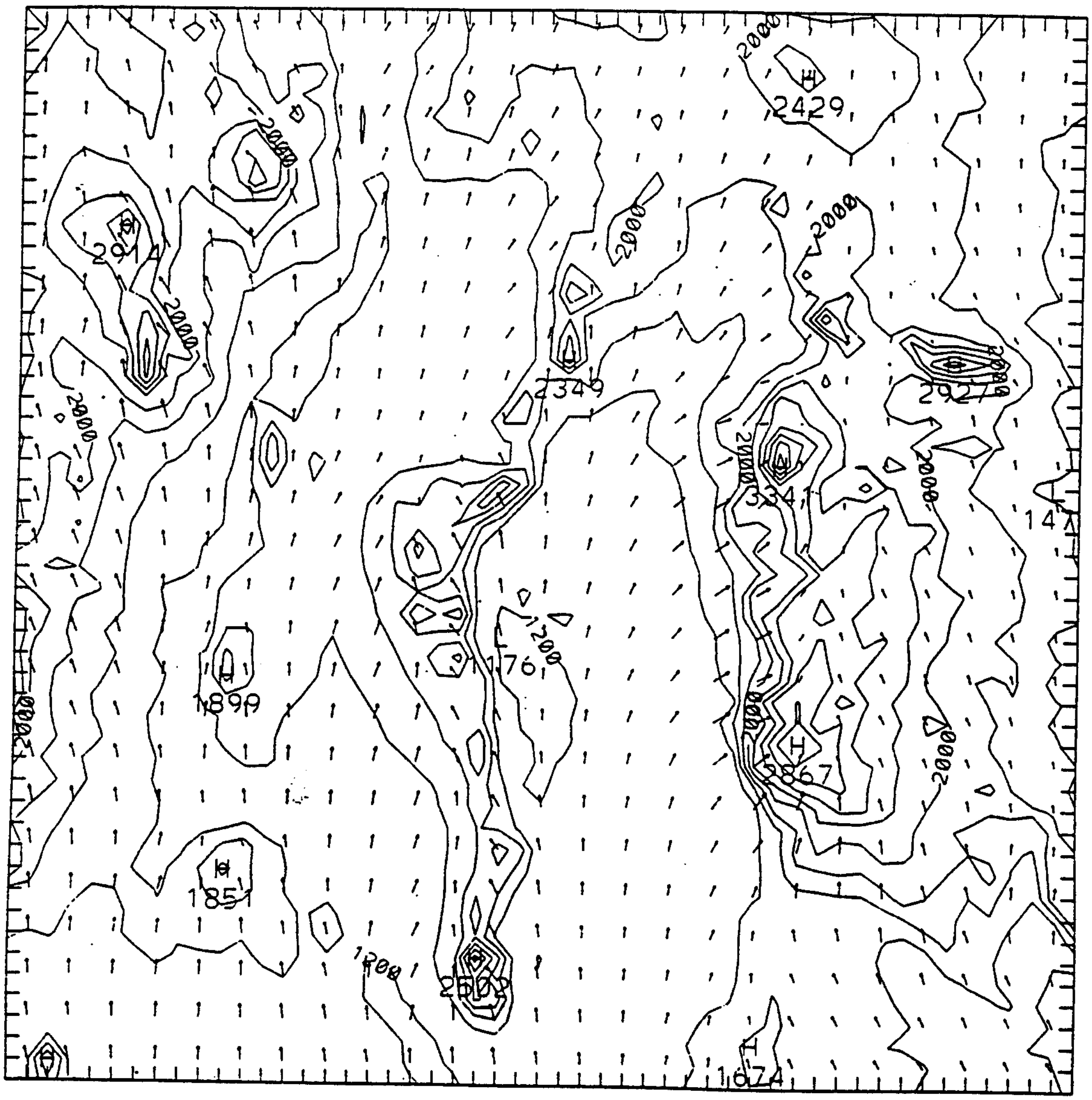

Figure 15. Forecast surface wind field at 17 LST on 10 Mar 94, maximum wind speed is 8.26 m/s. Initial wind field at 5 LST was calculated using mean speed and direction of SAMS stations.

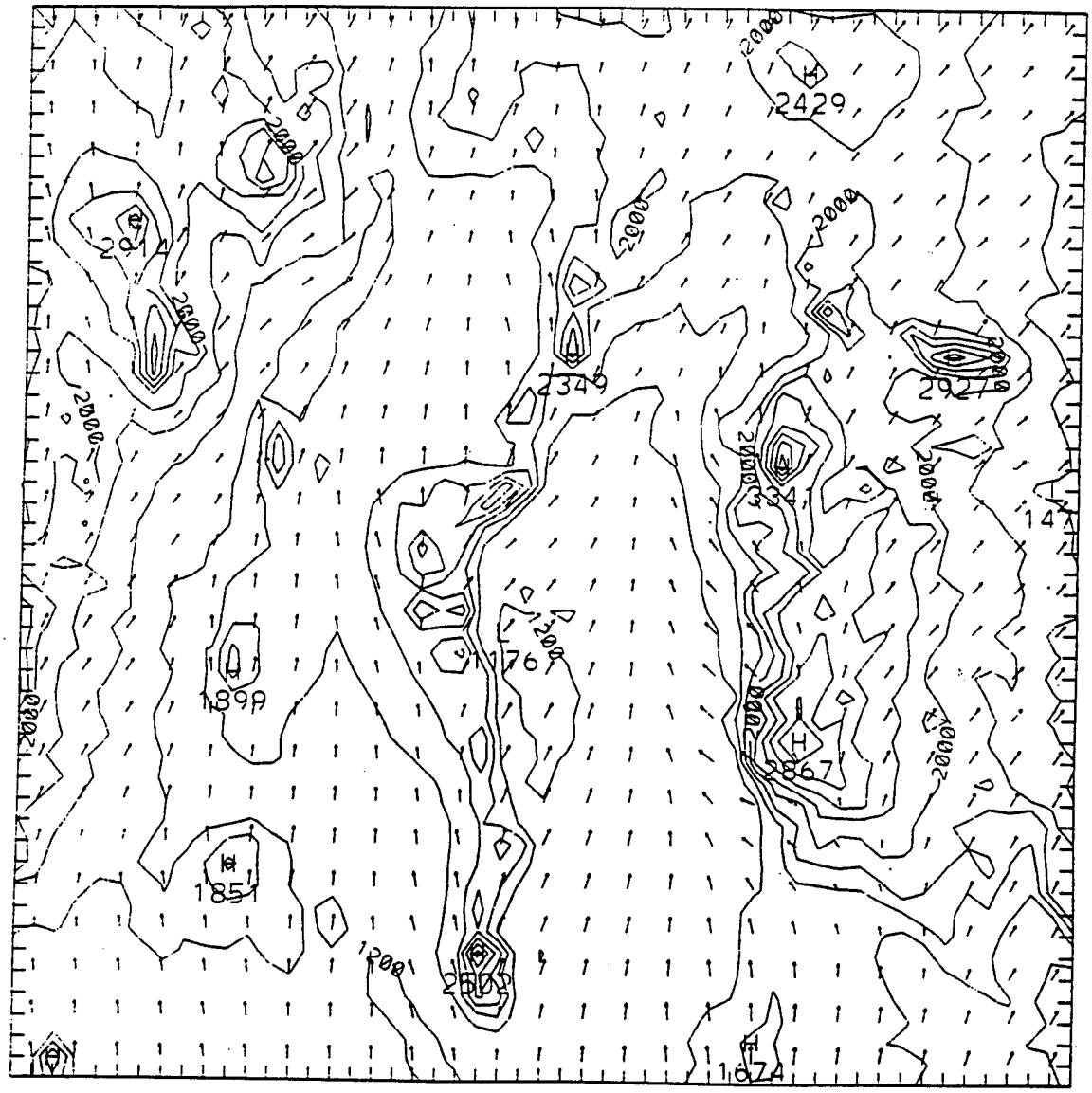

Figure 16. Forecast surface wind field at 7 LST on 10 Mar 94, maximum wind speed is 6.82 m/s. Initial wind field was calculated from GSM data.

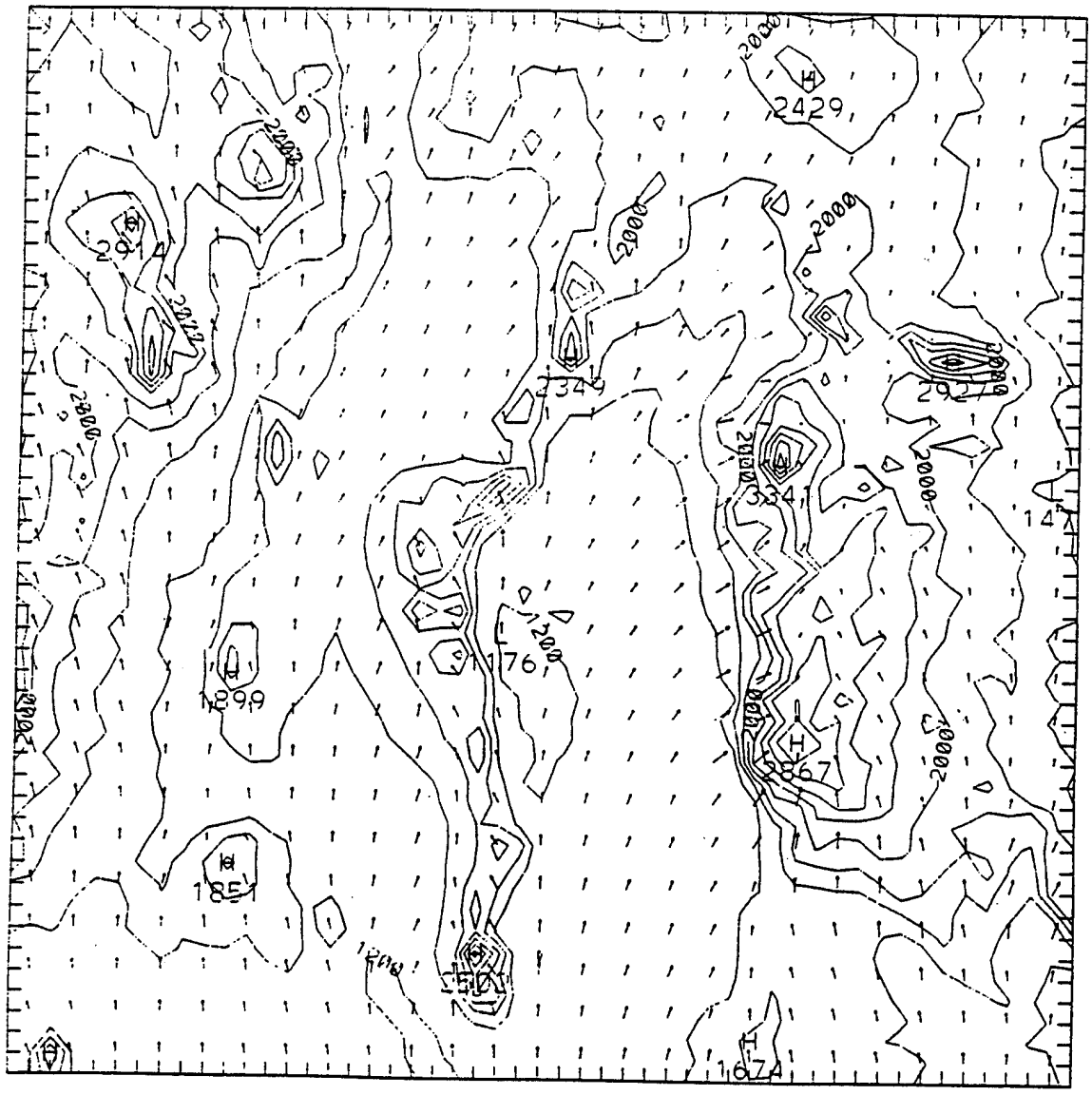

Figure 17. Forecast surface wind field at 10 LST on 10 Mar 94, maximum wind speed is 7.53 m/s. Initial wind field was calculated from GSM data.

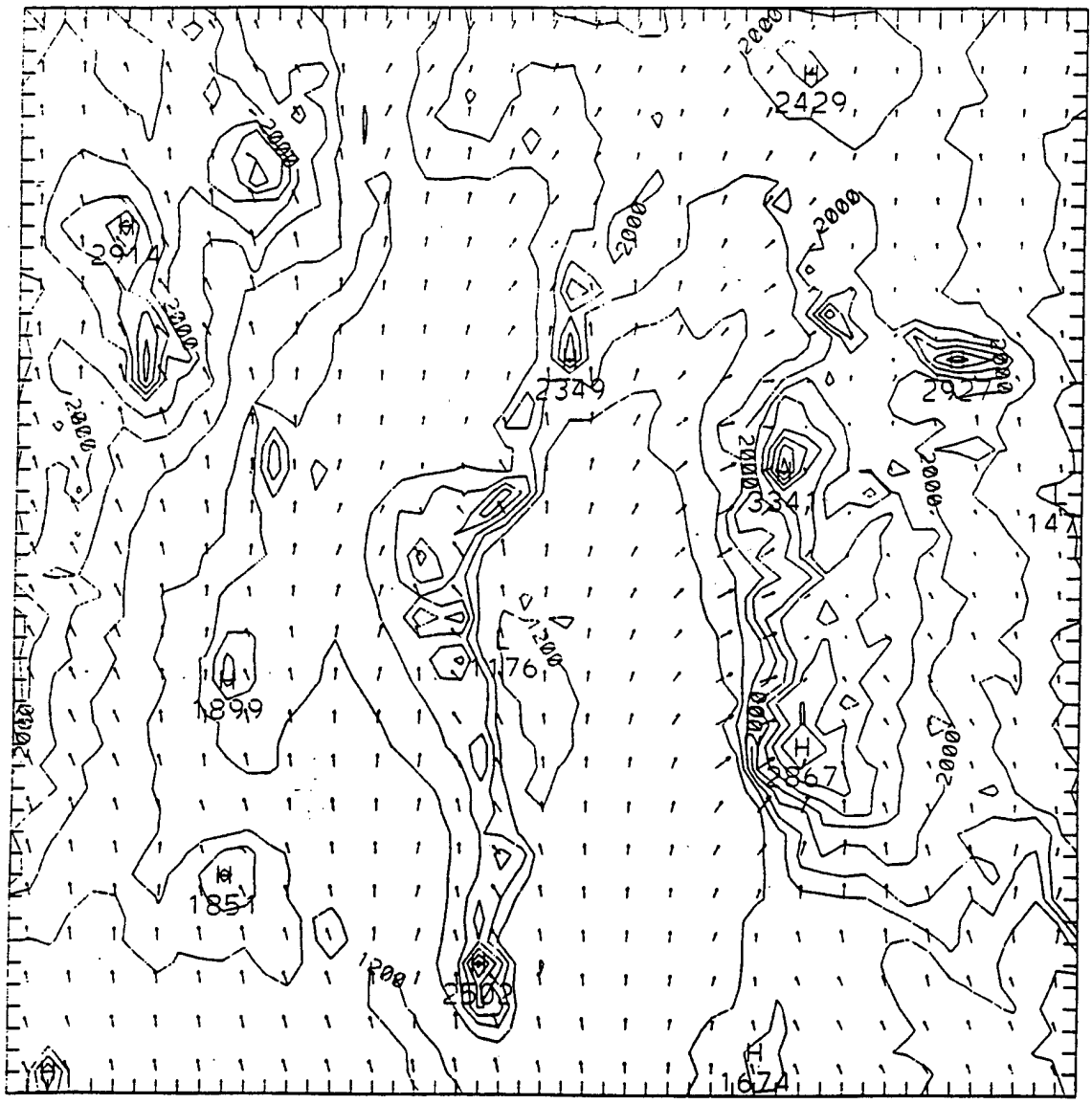

Figure 18. Forecast surface wind field at 11 LST on 10 Mar 94, maximum wind speed is 9.76 m/s. Initial wind field was calculated from GSM data.

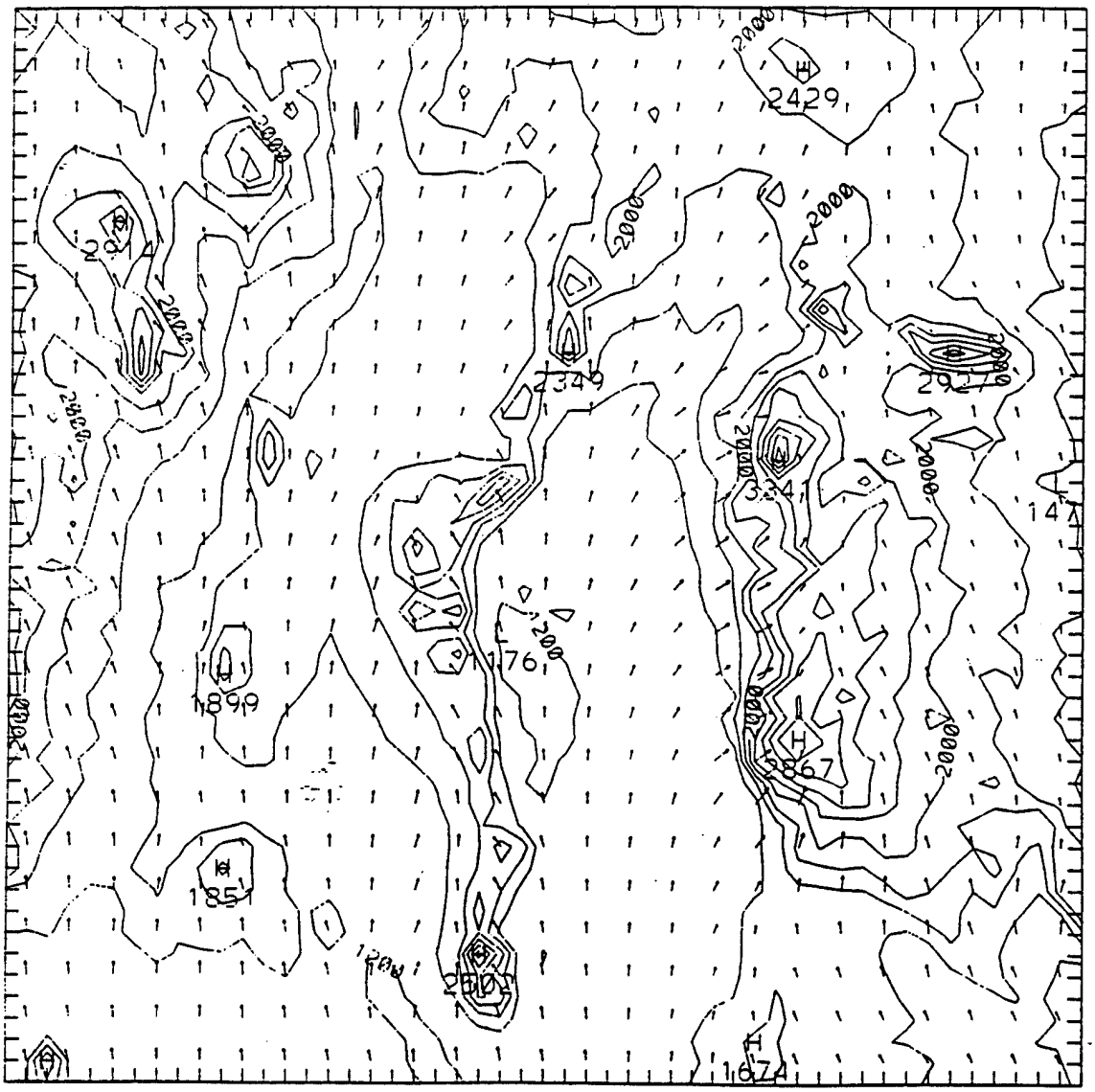

Figure 19. Forecast surface wind field at 17 LST on 10 Mar 94, maximum wind speed is 11.7 m/s. Initial wind field was calculated from GSM data.

Figures 20 through 23 show the 12-h variations of wind direction and speed at 10 m level and surface and dew-point temperature at 2 m level at four representative SAMS sites for the period of 5 through 17 LST on 10 Mar 94. Figure 2 shows the locations of SAMS. In the figures, solid lines represent calculation (forecast) and lines with circles represent observation. Stations 01 (CST) and 11 (DEN) are located in the Tularosa Valley and stations 09 (SAL) and 17 (SAC) are located, respectively, on the San Andres and Sacramento mountains.

Figures 24 through 27 are similar to figures 20 through 23, except that forecast calculation was initialized by the GSM data. Figures 24 through 27 again show that the initialization of forecast calculation by the GSM data failed to produce the northerly wind directions in the morning hour.

Figures 20 through 27 show that temperature and dew-point variations also are significantly different between the two different initialization methods. In both methods, identical sets of 3-D data of temperature and water vapor mixing ratio, analyzed from the GSM data, were assimilated into the model calculation.

Vertical distributions of horizontal u and v wind components and temperature are compared between the forecast calculation and the profiler observation. The location of the profiler is near 19 in figure 2. Figures 28 and 29 show the vertical distributions respectively, at 7 and 17 LST on 10 Mar 94. The model was initialized by the wind field shown in figure 11. Figures 30 and 31 are similar to figures 28 and 29, but they are initialized using the GSM data. From the comparisons between figures 28, 29, 30, and 31, excellent agreement between calculation and observation was obtained at 07 LST when the model was initialized using surface wind data, particularly, in the y-component of wind in the boundary layer. However, the two different initialization methods yielded very small discrepancies at 17 LST, as can be seen in figures 29 and 31. Because the nudging was made in both methods toward the same GSM data field at a 12-h forecast time, this result could have been expected.

It can be concluded from this case study that incorporation of observed wind data into the initialization field improves the wind field at early hours of forecast calculation.

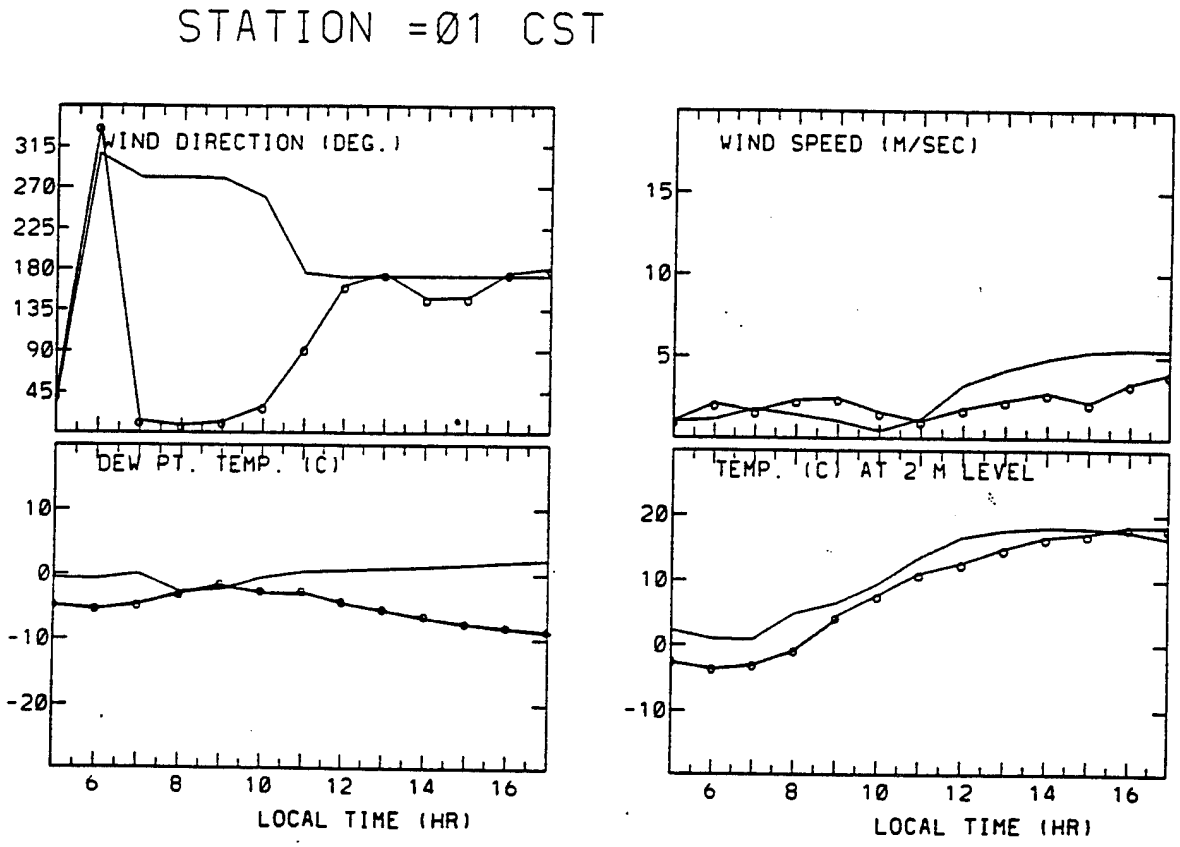

Figure 20. Temporal variations of wind direction and speed, dew point, and temperature at SAMS site 01 (CST). Solid lines represent forecast results, and lines with circles represent observation. Forecast calculation was initialized using mean wind speed and direction of SAMS stations.

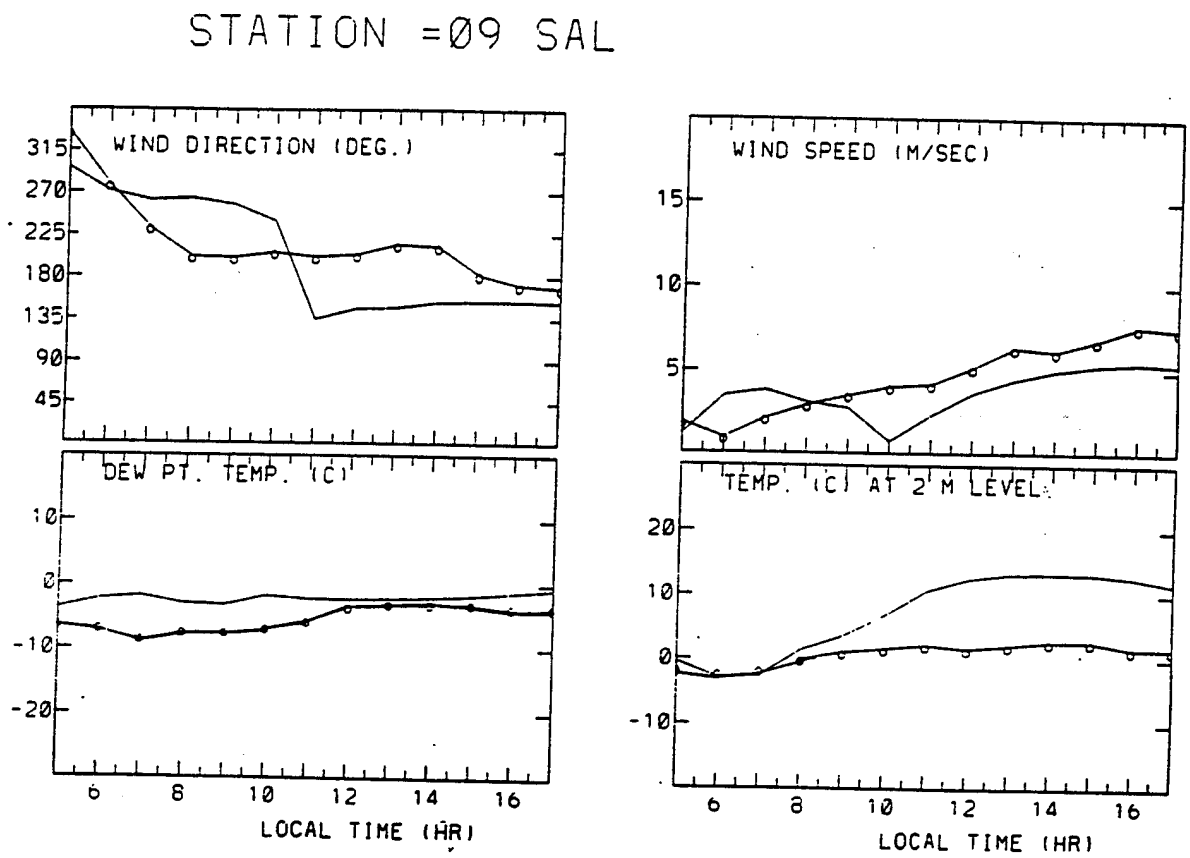

Figure 21. Temporal variations of wind direction and speed, dew point, and temperature at SAMS site 09 (SAL). Solid lines represent forecast results, and lines with circles represent observation. Forecast calculation was initialized using mean wind speed and direction of SAMS stations.

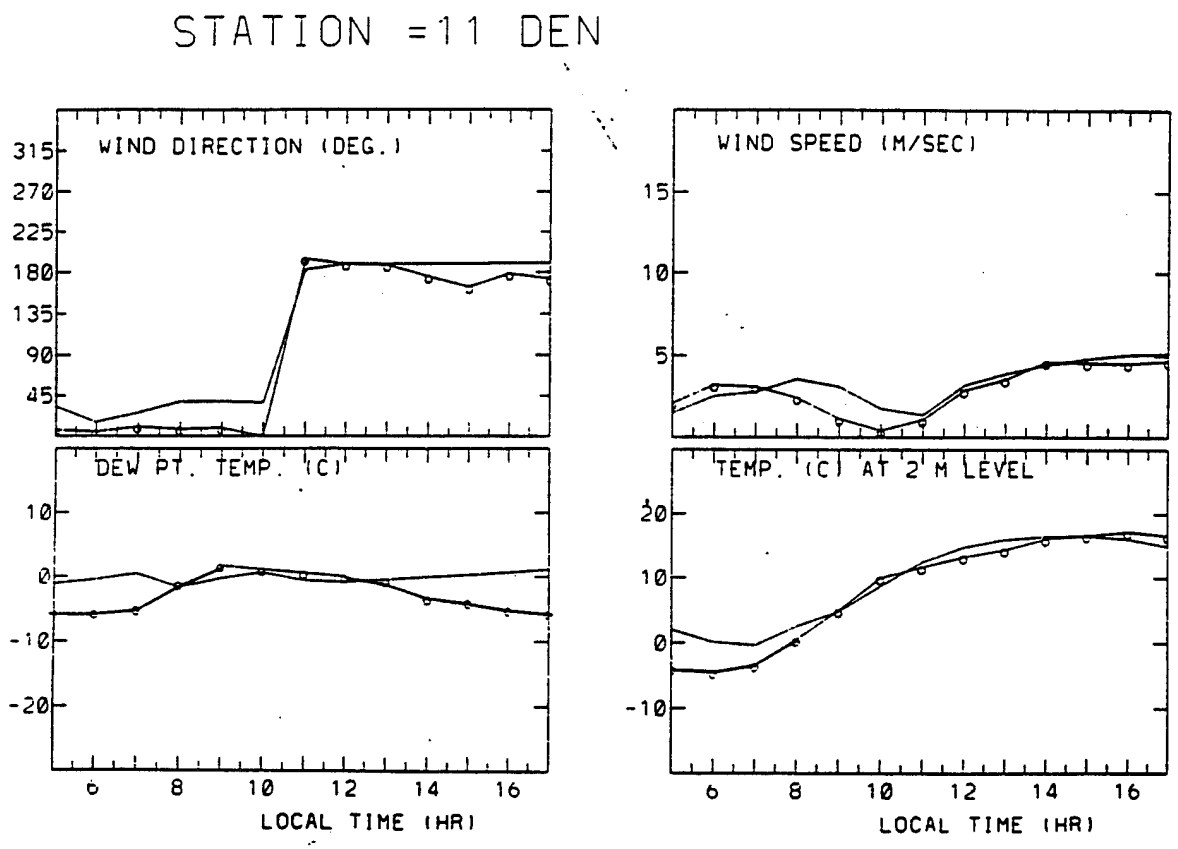

Figure 22. Temporal variations of wind direction and speed, dew point, and temperature at SAMS site 11 (DEN). Solid lines represent forecast results, and lines with circles represent observation. Forecast calculation was initialized using mean wind speed and direction of SAMS stations.

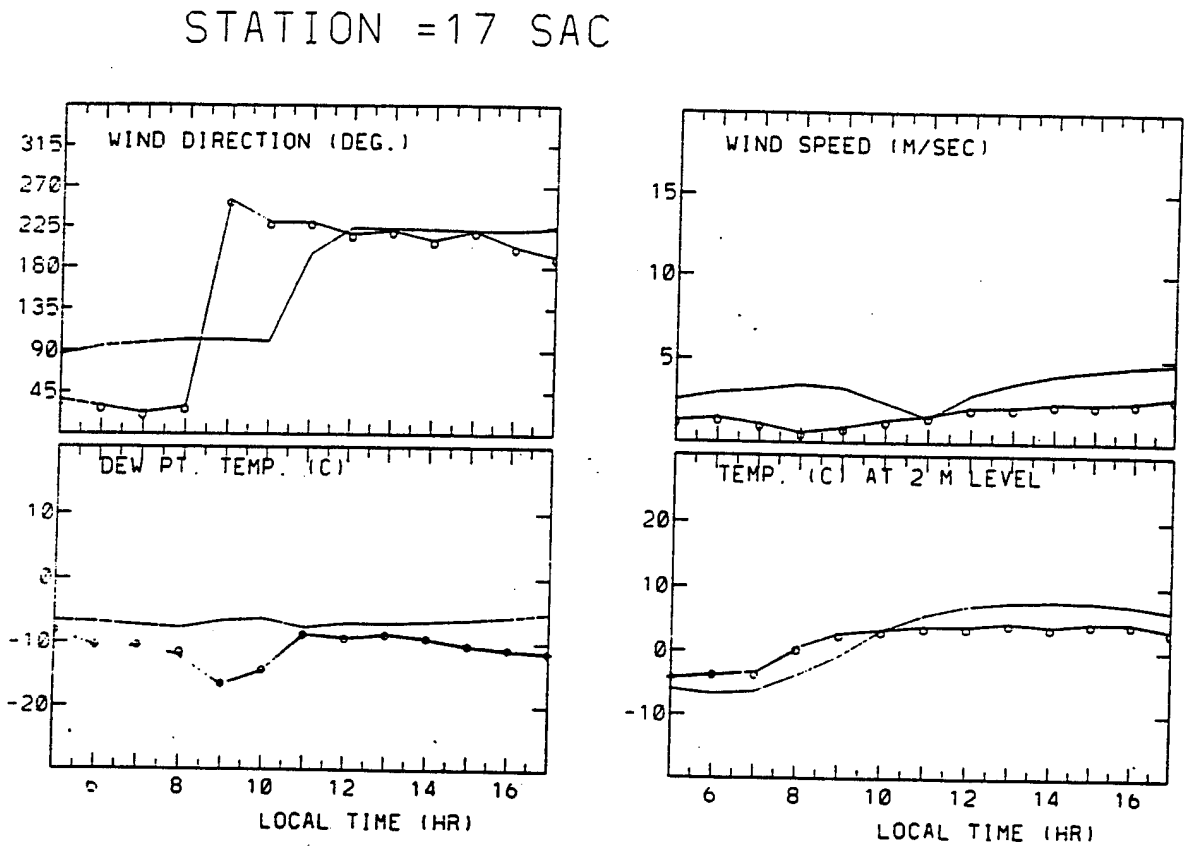

Figure 23. Temporal variations of wind direction and speed, dew point, and temperature at SAMS site 17 (SAC). Solid lines represent forecast results, and lines with circles represent observation. Forecast calculation was initialized using mean wind speed and direction of SAMS stations.

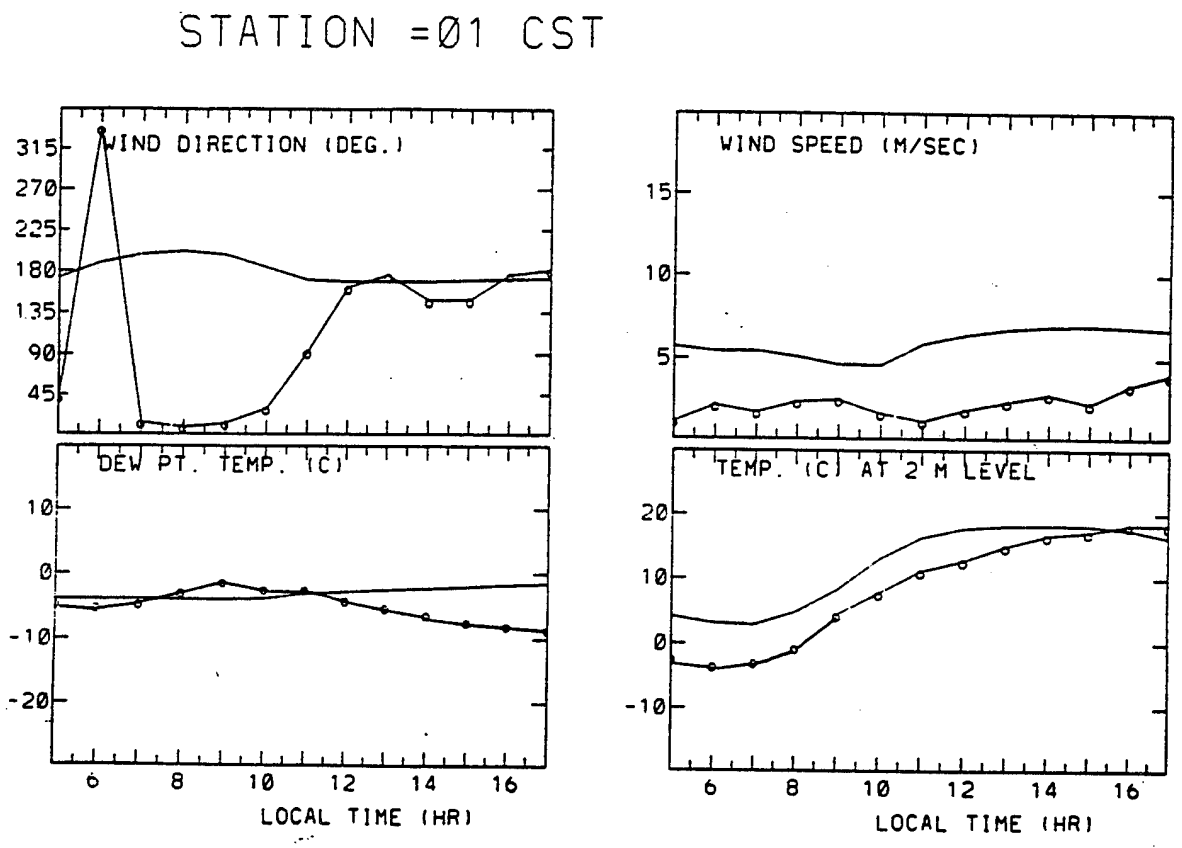

Figure 24. Temporal variations of wind direction and speed, dew point, and temperature at SAMS site 01 (CST). Solid lines represent forecast results, and lines with circles represent observation. Forecast calculation was initialized using GSM data.

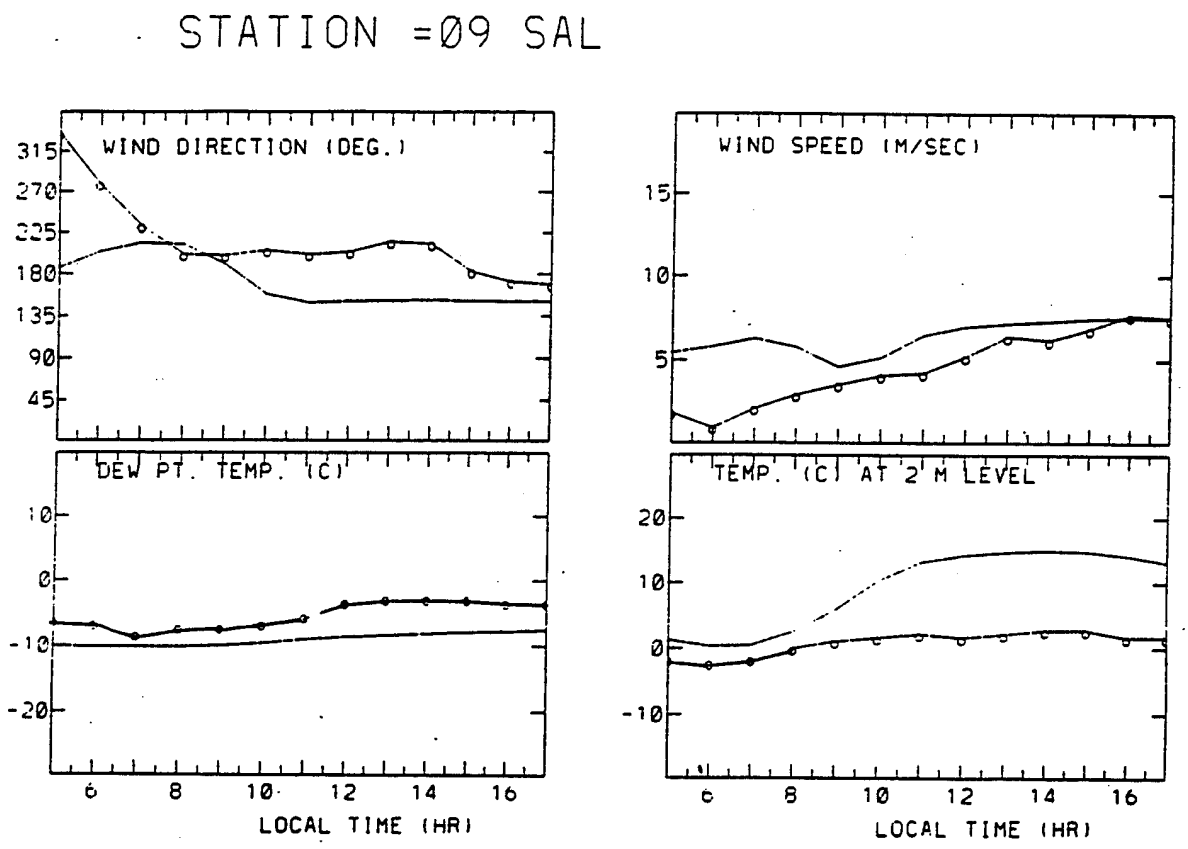

Figure 25. Temporal variations of wind direction and speed, dew point, and temperature at SAMS site 09 (SAL). Solid lines represent forecast results, and lines with circles represent observation. Forecast calculation was initialized using GSM data.

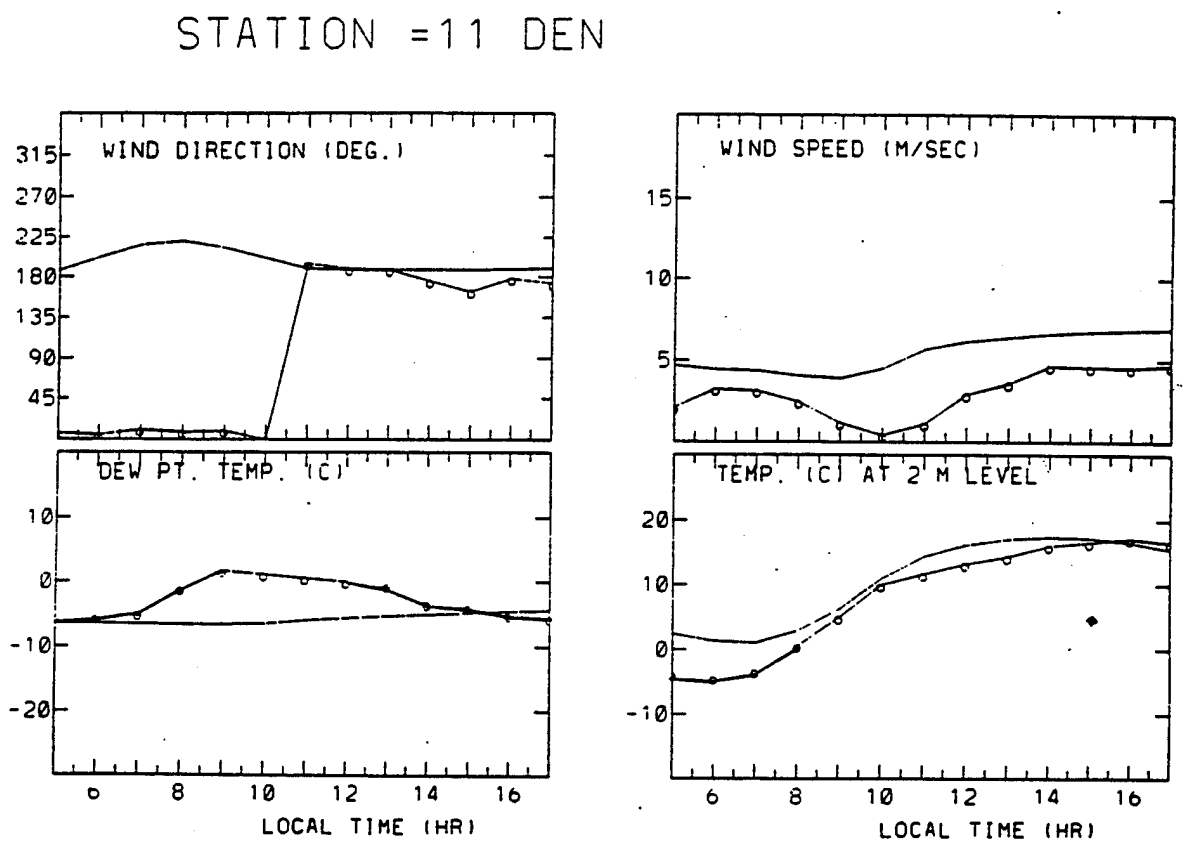

Figure 26. Temporal variations of wind direction and speed, dew point, and temperature at SAMS site 11 (DEN). Solid lines represent forecast results, and lines with circles represent observation. Forecast calculation was initialized using GSM data.

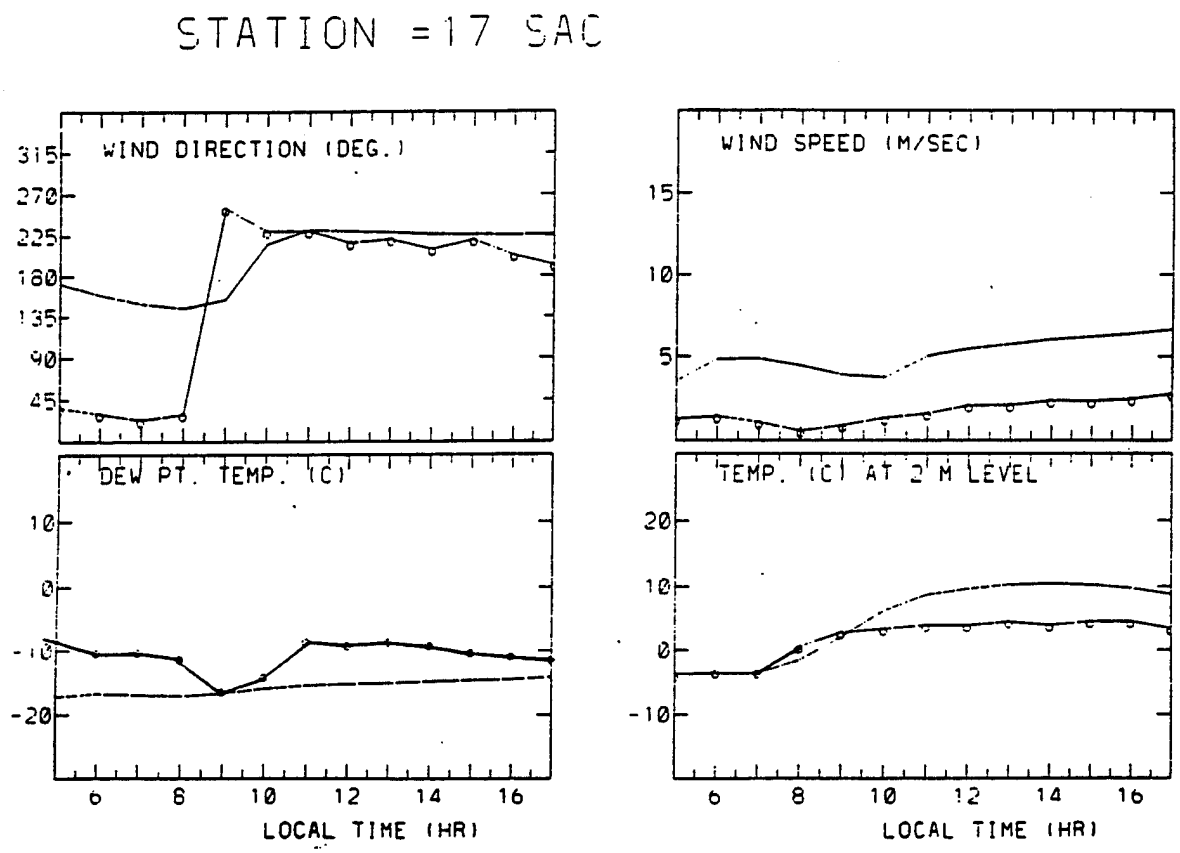

Figure 27. Temporal variations of wind direction and speed, dew point, and temperature at SAMS site 17 (SAC). Solid lines represent forecast results, and lines with circles represent observation. Forecast calculation was initialized using GSM data.

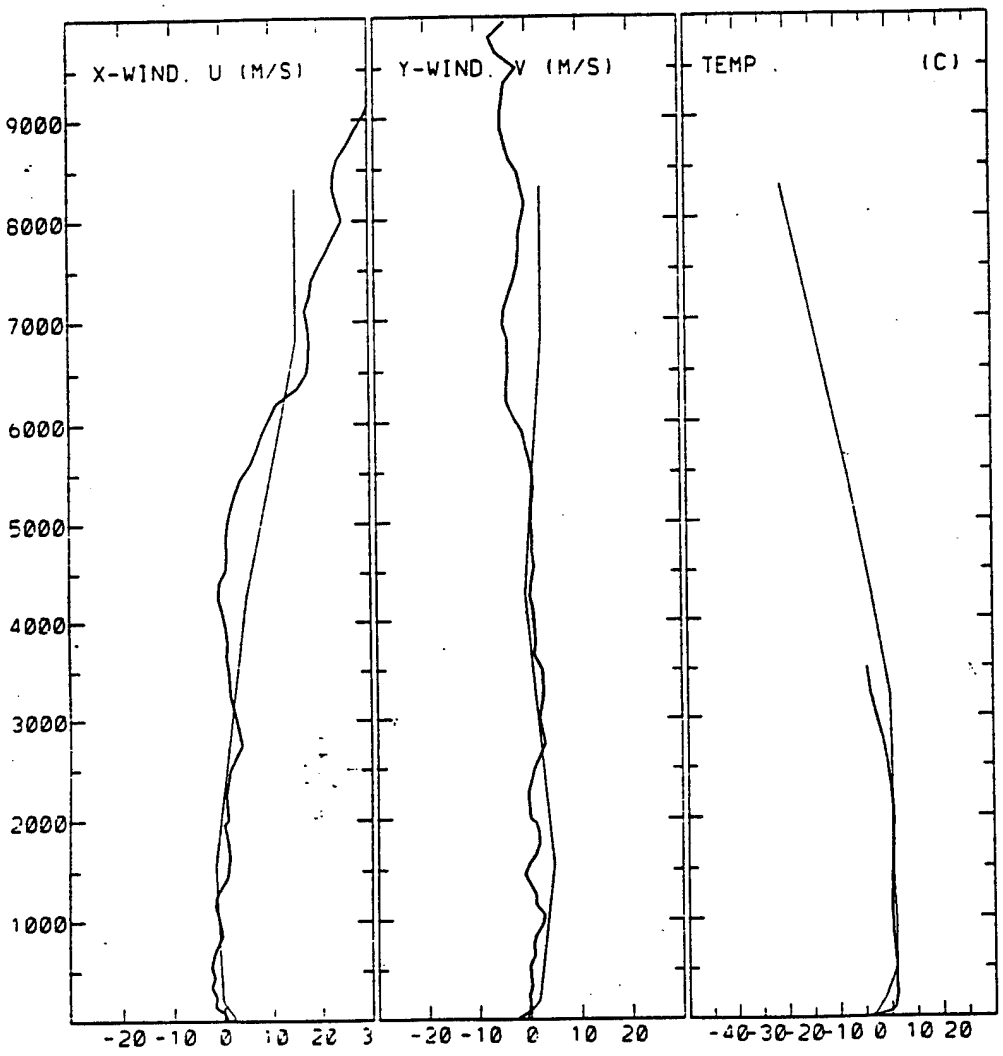

Figure 28. Vertical profiles of horizontal wind components u and v and temperature at 7 LST on 10 Mar 94. Thin lines represent forecast calculations, and thick lines represent observation. Forecast calculation was initialized using mean wind speed and direction, calculated from SAMS data at 05 LST.

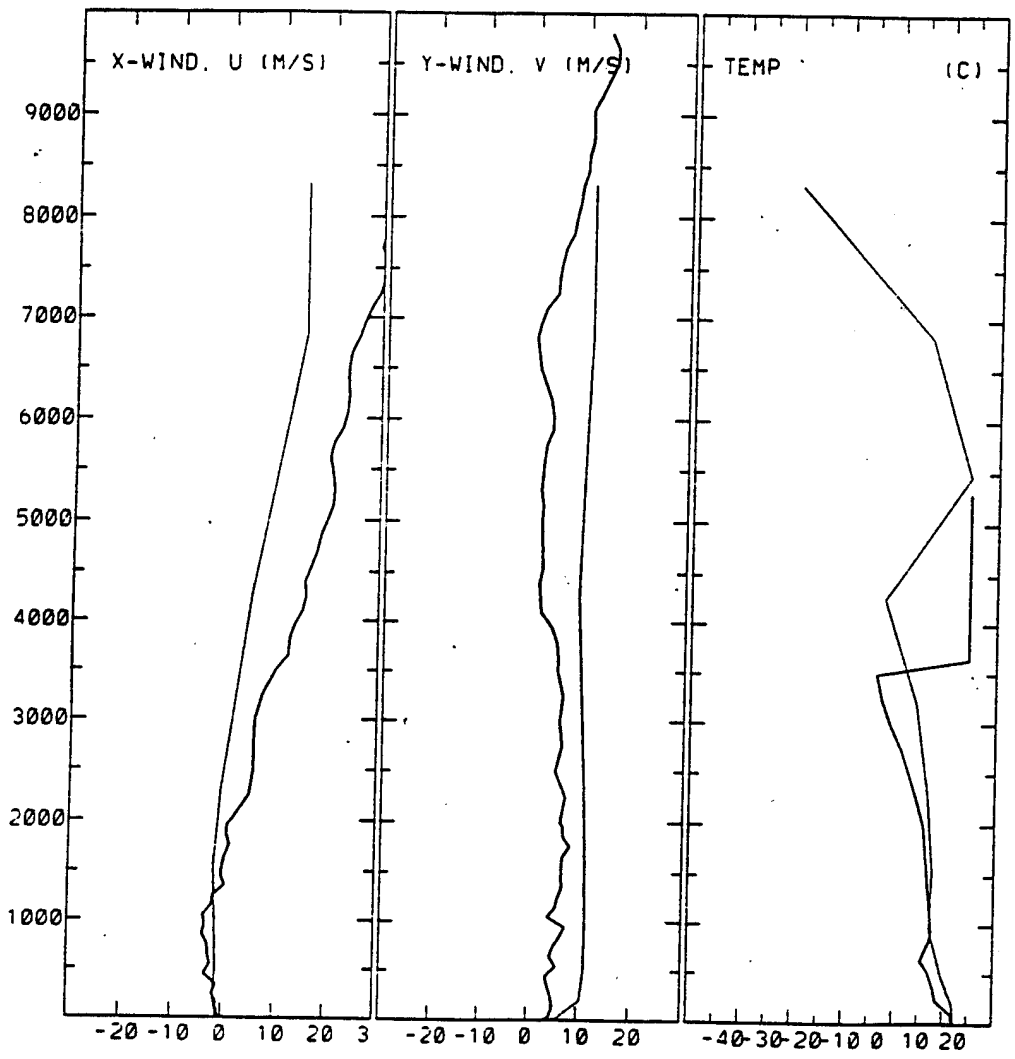

Figure 29. Vertical profiles of horizontal wind components u and v and temperature at 17 LST on 10 Mar 94. Thin lines represent forecast calculations, and thick lines represent observation. Forecast calculation was initialized using mean wind speed and direction, calculated from SAMS data at 05 LST.

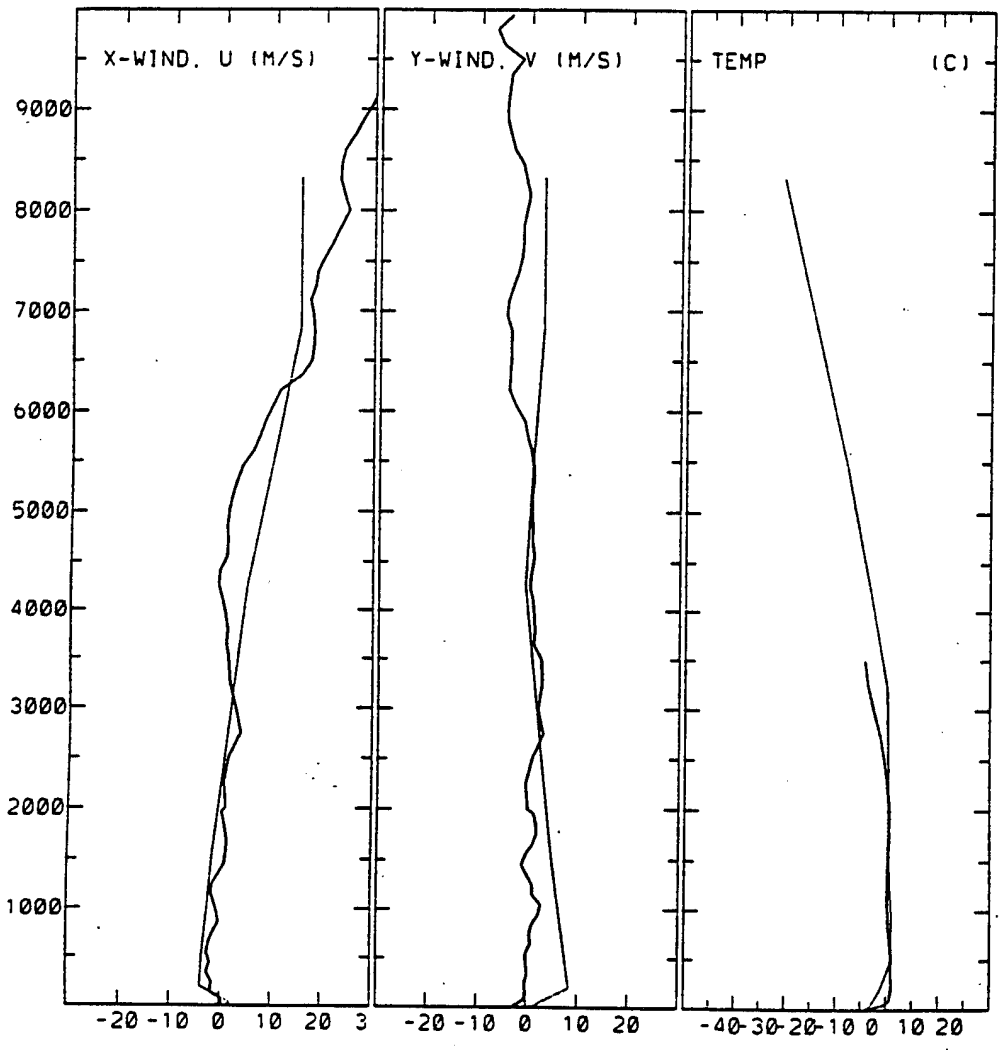

Figure 30. Vertical profiles of horizontal wind components u and v and temperature at 7 LST on 10 Mar 94. Thin lines represent forecast calculations, and thick lines represent observation. Forecast calculation was initialized using GSM data at 05 LST.

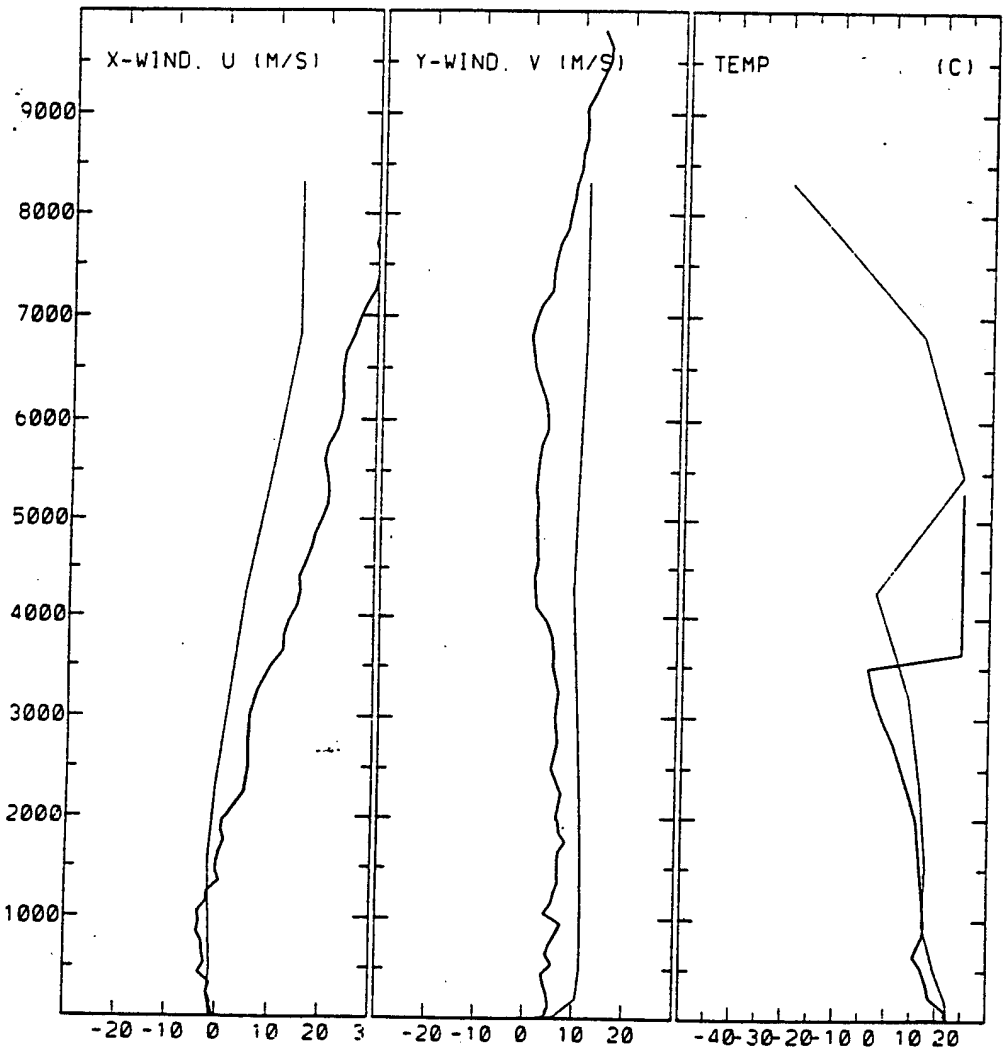

Figure 31. Vertical profiles of horizontal wind components u and v and temperature at 17 LST on 10 Mar 94. Thin lines represent forecast calculations, and thick lines represent observation. Forecast calculation was initialized using GSM data.

5. Initialization Methods

Based on the study described in section 4, the BFM was initialized by three different methods described in sections 5.1 through 5.3. Horizontal wind components u and v and temperature were compared with observations at every hour of the forecasting periods. For the comparison, two additional computed data mentioned in sections 5.4 and 5.5 were also compared with observations.

5.1 Initialization Using GSM

The GSM uses normalized pressure, sigma = p/p_s, for a vertical coordinate. Thus, meteorological variables are calculated on constant pressure surfaces. The GSM analyses and 12-h forecast values of horizontal wind components, temperature, dew-point depression, and geopotential height on mandatory pressure levels are used in this study.

HOTMAC uses z^*, defined in the following manner, for a vertical coordinate:

$$z^* = \overline{H}\frac{z - z_g}{H - z_g} \tag{11}$$

where

z^* = the transformed vertical coordinate
z = the Cartesian vertical coordinate
z_g = ground elevation above sea level
$\overline{H}$ = the material surface top of the model
H = the corresponding height in the Cartesian coordinate.

H is defined as

$$H = \overline{H} + z_{gmax} \tag{12}$$

where

z_{gmax} = the maximum value of z_g.

Because different vertical coordinates are used in GSM and HOTMAC, the following two procedures are performed to format GSM output data to initialize HOTMAC:

1. Horizontal interpolations of wind components (u,v), temperature, mixing ratio, and geopotential height from GSM grid points to HOTMAC grid points on constant pressure surface; Barnes' method [12] is used for horizontal interpolation.

2. A linear interpolation method is used for vertical interpolations of the variables from constant pressure to z^* surfaces at HOTMAC grid points.

For 12-h forecasts, current analyses and 12-hr forecast fields of GSM are analyzed using the above method, and hourly data are generated by a linear interpolation between two time periods. At 1 h before the initiation of forecast computation, the first hourly analyses field data are assimilated using the nudging method for 1 h. After that, the next hourly data are assimilated in at 1 h ahead of forecast time for 1 h. This process is repeated for the entire 12-h period.

In this study, nudging was enforced only in the 9 uppermost layers (corresponding to a height greater than 151 m of z^*) of 16 vertical layers.

5.2 Initialization Using GSM and Mean Surface Wind Direction and Speed

As described in section 4, wind directions in the layers near the surface reduced from GSM data are sometimes significantly different from those observed. Thus, to obtain good agreements of wind vectors between computation and observation in short-range forecasts, incorporation of surface wind data into initial fields is necessary. From SAMS data, mean surface wind vector components were calculated at the initial forecast time, and logarithmic wind profiles are assumed from the surface (z^* = 10 m) to the seventh layer (z^* = 151 m) as

$$V_{obs}(k) = -WS_{obs}\cos(\theta_{obs})\log\frac{z^*(k)}{z^*(4)} \quad (13)$$

$$U_{obs}(k) = -WS_{obs}\sin(\theta_{obs})\log\frac{z^*(k)}{z^*(4)} \quad (14)$$

For the eighth and ninth layers, linear interpolations of vector components (u,v) are made as

$$U_{obs}(k) = U_{obs}(7) + \frac{U_{obs}(10) - U_{obs}(7)}{z^*(10) - z^*(7)}(z^*(k) - z^*(7)) \quad (15)$$

$$V_{obs}(k) = V_{obs}(7) + \frac{V_{obs}(10) - V_{obs}(7)}{z^*(10) - z^*(7)}(z^*(k) - z^*(7)) \quad (16)$$

where

WS_{obs}	=	mean surface wind speed
θ_{obs}	=	mean surface wind direction
$U_{obs}(k)$	=	x component of wind vectors at the kth layer
$V_{obs}(k)$	=	y component of wind vectors at the kth layer
$U_{obs}(10)$	=	10th layer wind components calculated from the GSM data
$V_{obs}(10)$	=	10th layer wind components calculated from the GSM data

5.3 Nudging of Individual Surface Wind Data at Initial Time

In addition to the method in 5.2, individual wind data obtained at initialization time were assimilated into model calculations at the grid points adjacent to the SAMS locations.

The method of assimilation of surface wind data is as follows:

$$U_{obs}(i,j) = \frac{\sum_l (\frac{U_l}{r_l^2})}{\sum_l (\frac{1}{r_l^2})} \tag{17}$$

Wind vector components at grid point (i,j) at the fourth layer ($z^* = 10$ m) are calculated as

$$V(i,j) = \frac{\sum_l (\frac{V_l}{r_l^2})}{\sum_l (\frac{1}{r_l^2})} \tag{18}$$

where

U_l = the x component of the wind vector at station l
V_l = the y component of the wind vector at station l
r_l = the grid distance between station l and a grid point (i,j).

The nudging parameter at a grid point (i,j) for $r < R$ is calculated as

$$c_l = a_l (1.0 - \frac{r_l^2}{R^2}) \tag{19}$$

where

a_l = an empirical constant (0.01).

For $r \geq R$,

$$c_l = 0.0 \tag{20}$$

where

R = a critical distance.

Grid points located within a grid distance less than 4 were assumed affected by the nudging of GSM data.

5.4 Surface Data Nudging Every 3 h

The method in section 5.3 nudges wind data only at the first hour of model computation. In this method, the SAMS wind data is assimilated into model calculations every 3 h. The data observed at 5, 8, 11, 14, and 17 LST were nudged from 4, 7, 10, 13, and 16 LST for 1 h.

5.5 Linear Interpolation of GSM Data

For comparison purposes, the 3-D GSM data set, created by the method described in section 5.1 at two time periods, is linearly interpolated in time. Resulting data at hourly intervals are compared with observations.

6. Statistical Parameters

To examine the differences in the results using methods described in sections 5.1 through 5.5, the following statistical parameters are calculated hourly by using the data from the 25 different cases.

6.1 Mean Residual

The difference between observed and forecast values of a meteorological parameter can be written as follows:

$$F_{res} = F_{obs} - F_{for} \tag{21}$$

where

F = a meteorological parameter.

The subscripts (res), (obs), and (for) represent residual, observation, and forecast, respectively.

A mean residual for different forecast hours is defined as follows:

$$\overline{F_{res}}(t) = \frac{\sum_m \sum_n F_{res,m,n}(t)}{m \times n} \tag{22}$$

where

t = forecast time
m = the number of forecast cases
n = the number of SAMS data.

6.2 Standard Deviation of Residual

The standard deviation of residual of a meteorological parameter is defined as follows:

$$\sigma_{F_{res}}(t) = \pm\left(\frac{\sum_m \sum_n (F_{res,m,n}(t) - \overline{F_{res}}(t))^2}{m \times n}\right)^{\frac{1}{2}} \quad (23)$$

where

$F_{res}(t)$ = the standard deviation of the residual at forecast time t.

Improved forecast calculations result in mean residuals converging to zero in conjunction with smaller standard deviations of residual. Perfect agreement between observation and forecast results in zero for both parameters.

7. Results

Twenty five cases given in table 1 were simulated using the different initialization methods described in section 5. Statistical parameters in the 25 cases were calculated for every hour of forecast calculation from 1 to 12 h.

In figures 32 through 36, the mean residuals (thick lines) and standard deviations (thin lines) are plotted as a function of time.

Comparisons of figures 32 through 36 reveal the following:

1. From figures 32 and 36, the BFM produced much better forecast fields of wind and temperature than the linear interpolation of GSM data. In general, the values of mean residuals and standard deviations are smaller in figure 32 than in figure 36. When the GSM data are input to the BFM, physical schemes of the model produced better agreement than simple interpolation of the data in time and space.

2. From figures 32 and 33, the initialization using the mean wind speed and direction (section 5.2) produced better forecast fields than the GSM data initialization (section 5.1). Substantial improvements in x and y components of wind vectors were obtained. As can be seen in figure 32, the mean residual values of both wind vector components were negative, meaning that BFM forecast calculations initialized by the GSM data produced larger wind vector components than the observed. Conversely, the mean residual values in figure 33 are much closer to zero, indicating that the average BFM, using mean wind speed and direction at initial times, produced surface wind vector component magnitudes similar to those observed. Even temperature mean residuals in figure 32 showed larger negative values throughout the 12-h forecast calculation than in figure 33. The initial temperature fields using the methods in sections 5.1 and 5.2 are identical for all 25 simulations. The model's schemes of boundary layer produce better temperature predictions using the method in section 5.2, compared to the method in section 5.1.

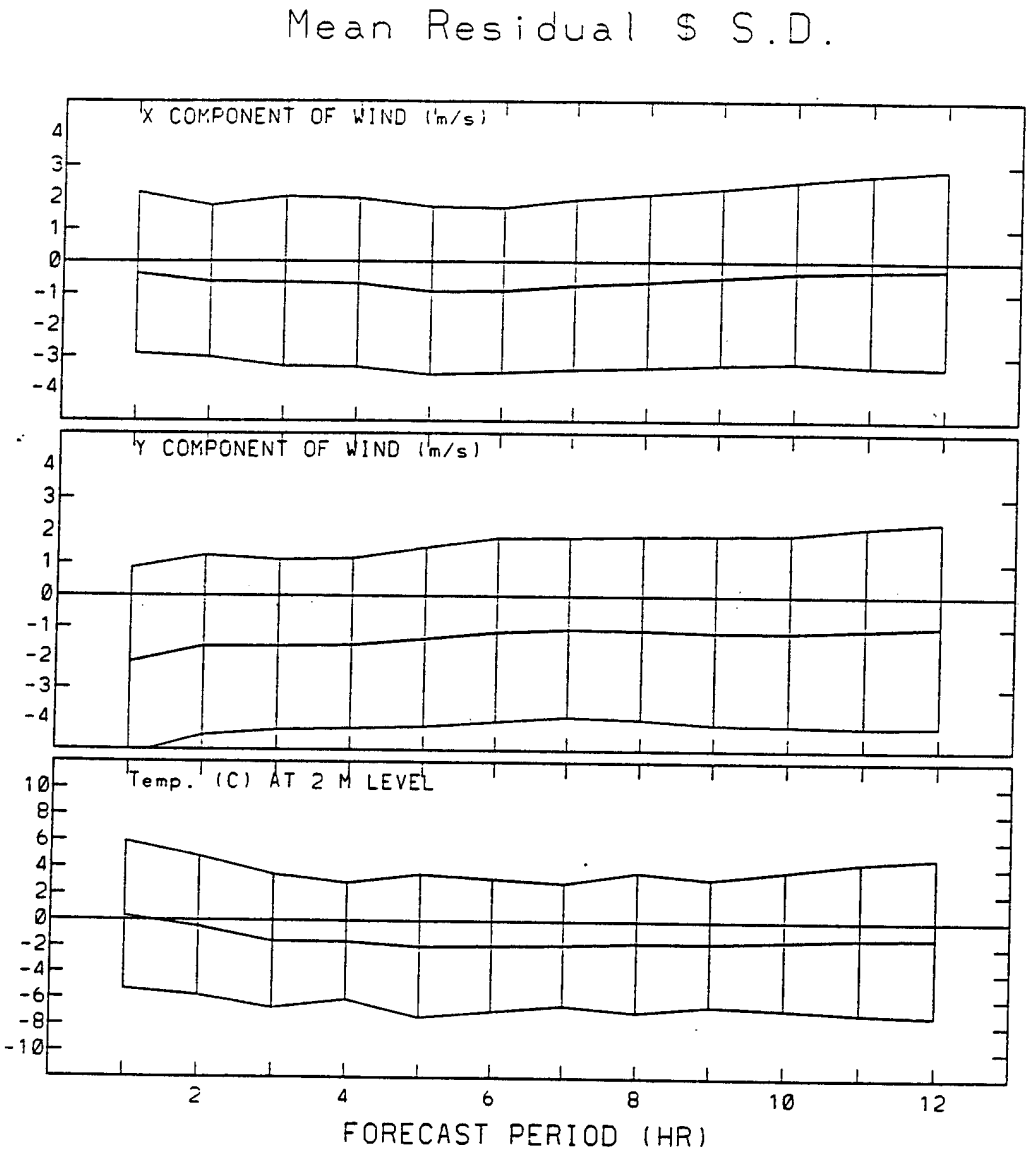

Figure 32. Temporal variations of mean residual (mean curves) and standard deviation (upper- and lower-bound curves) for the method in section 5.1 (initializing using GSM only). Upper plots represent the surface x wind vector components, middle plots are the y wind vector components, and bottom plots are surface temperature.

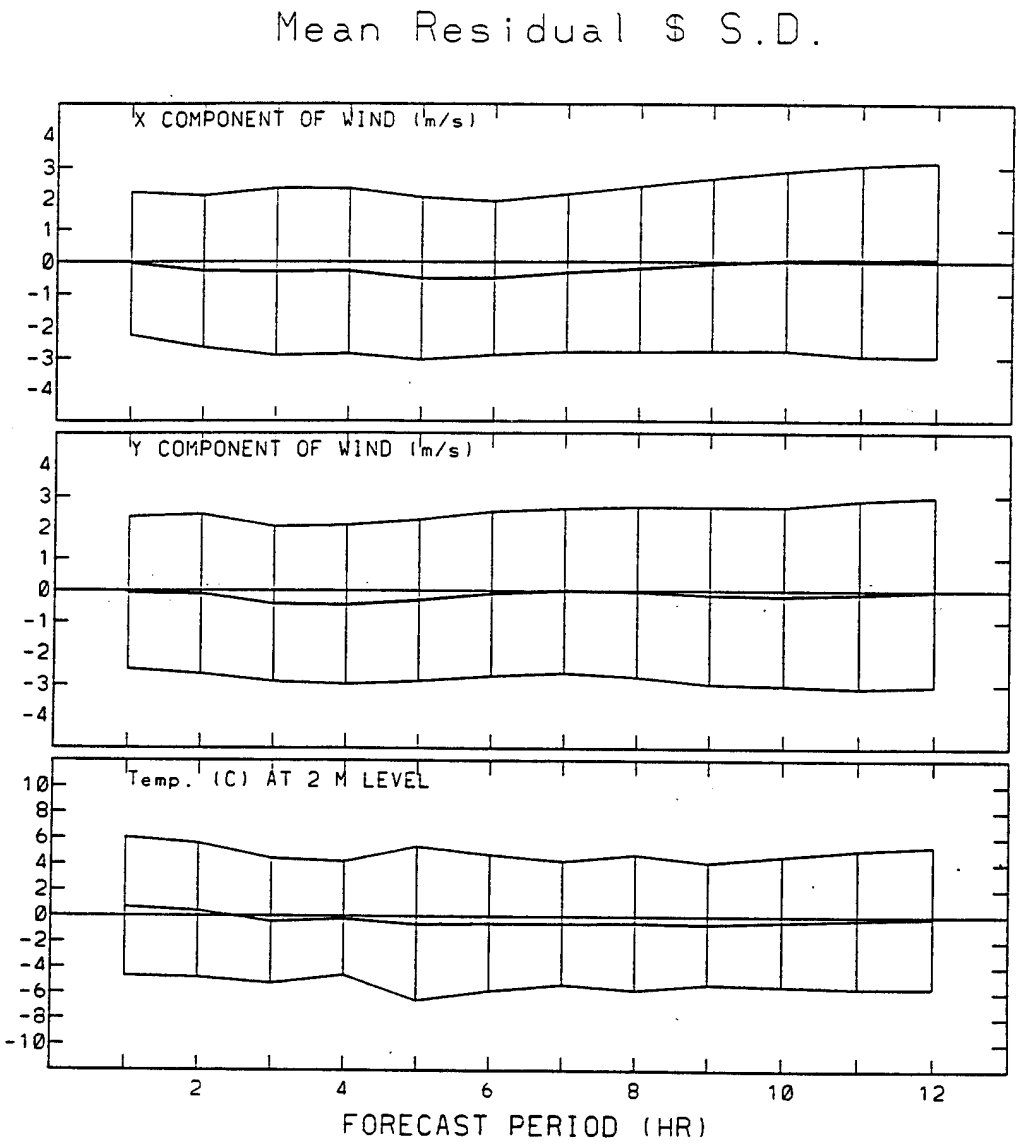

Figure 33. Temporal variations of mean residual (mean curves) and standard deviation (upper- and lower-bound curves) for forecast calculation initialized by the method in section 5.2 (initialization using GSM and mean surface wind direction and speed). Upper plots are the surface x wind vector components, middle plots are the y wind vector components, and bottom plots are surface temperature.

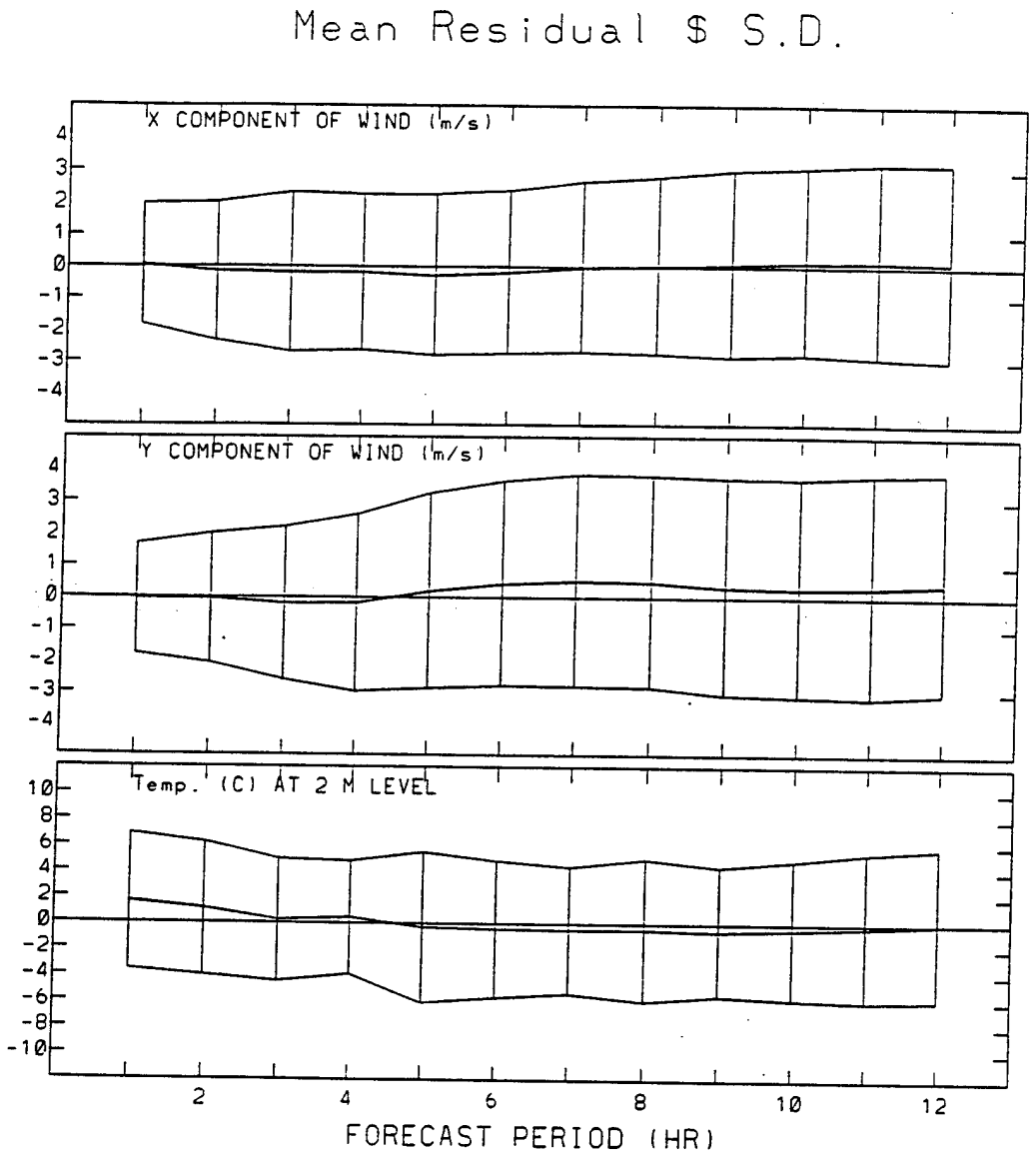

Figure 34. Temporal variations of mean residual (mean curves) and standard deviation (upper- and lower-bound curves) for forecast calculation initialized by the method in section 5.3 (initialization using GSM and mean surface wind direction and speed, plus nudging of individual surface data at initial time). Upper plots are the surface x wind vector components, middle plots are the y wind vector components, and bottom plots are surface temperature.

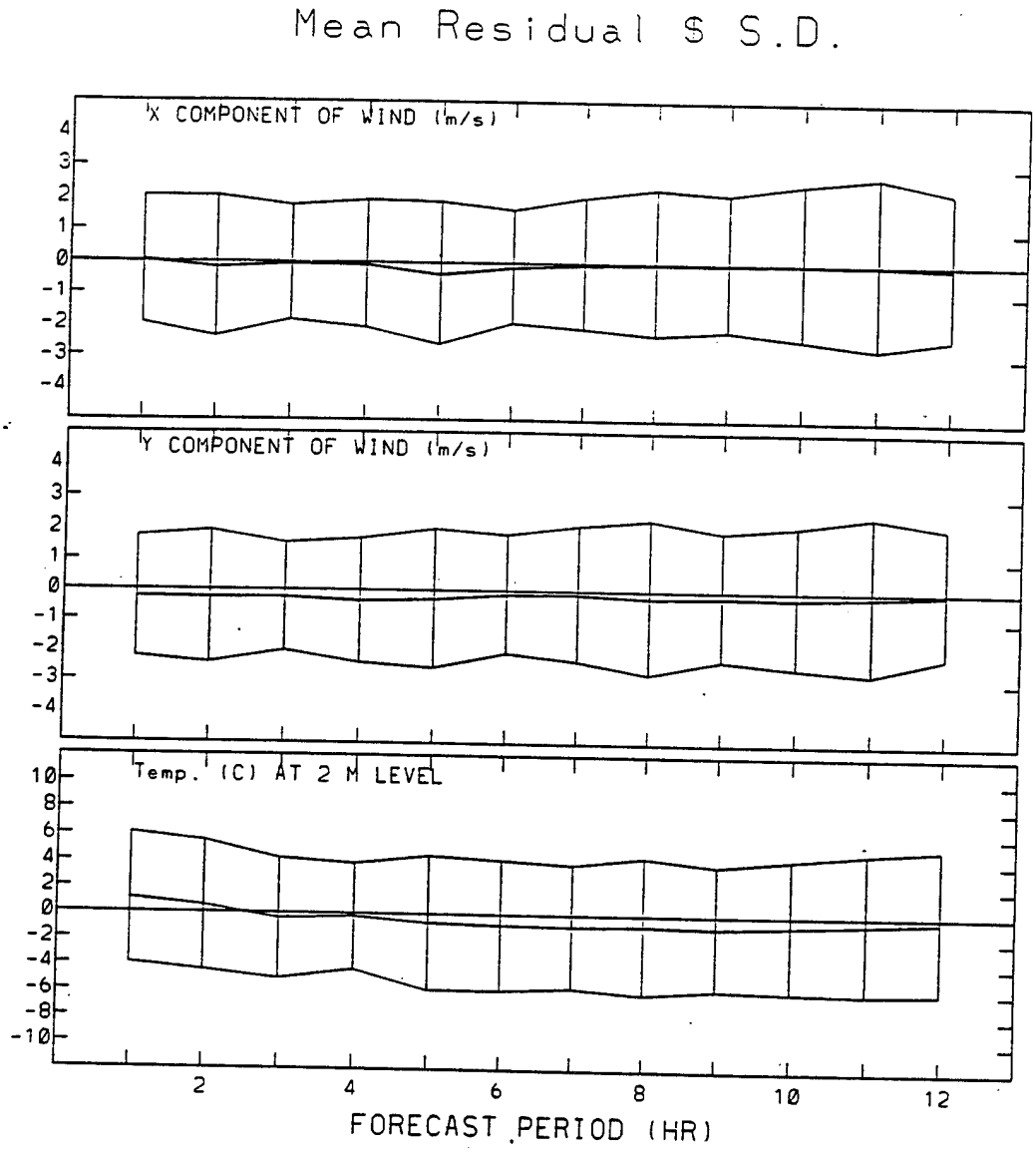

Figure 35. Temporal variations of mean residual (mean curves) and standard deviation (upper- and lower-bound curves) for surface wind data nudged every 3 h of calculation (section 5.4). Upper plots are the surface x wind vector components, middle plots are the y wind vector components, and bottom plots are surface temperature.

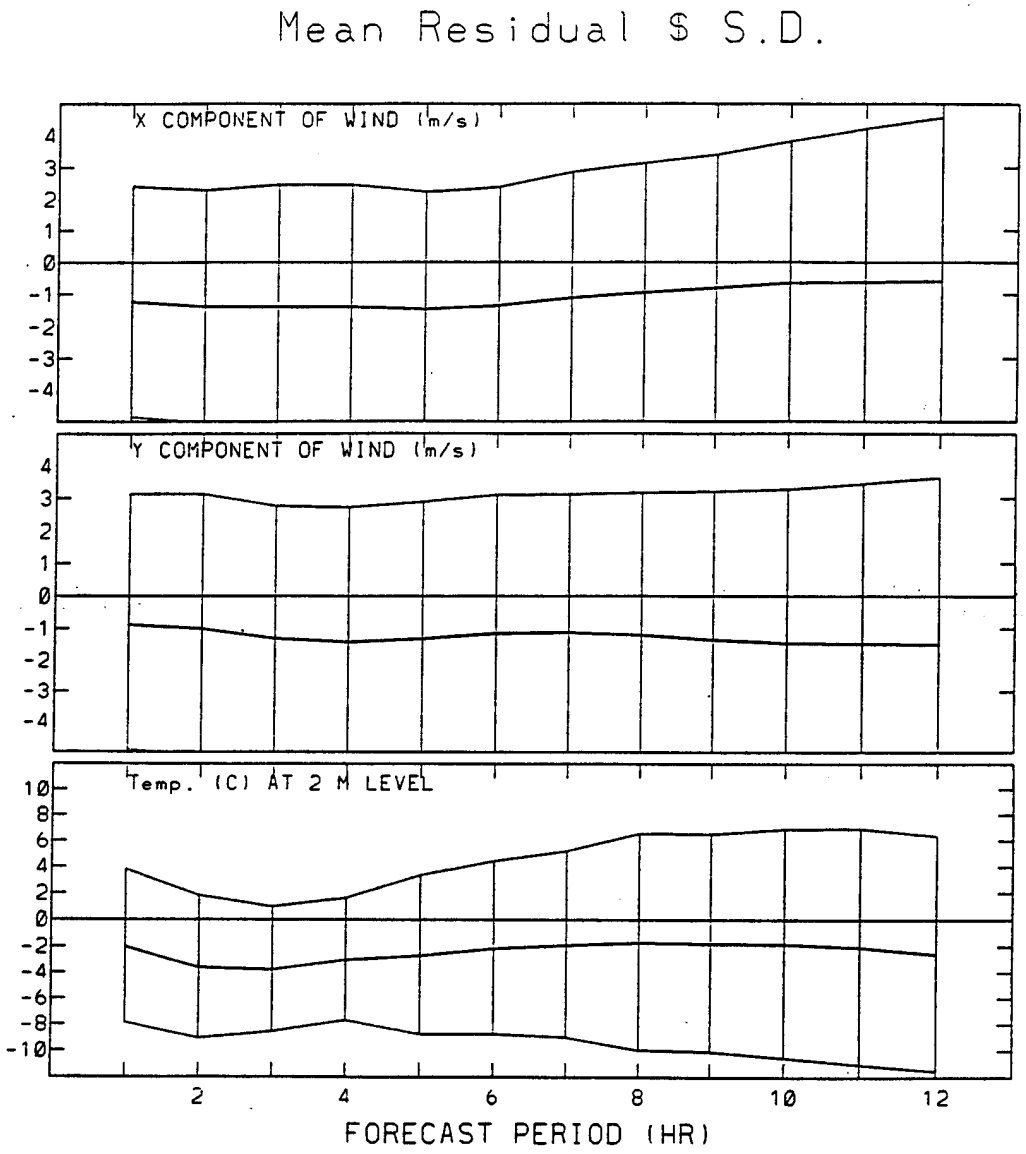

Figure 36. Temporal variations of mean residual (mean curves) and standard deviation (upper- and lower-bound curves) for temporal and spatial interpolation of GSM data. Upper plots are the surface x wind vector components, middle plots are the y wind vector components, and bottom plots are surface temperature.

Although it is not clearly understood, the profiles of wind components assumed in the method in section 5.2 may coincide to produce good temperature profile predictions in the boundary layer. Further studies are needed to understand this problem.

3. Comparison between figures 33 and 34 indicate that nudging the surface wind vector components at the forecast initial time (section 5.3) produced better forecast results in wind fields for a few hours of the early stage of calculation, but during the later stage of calculation, the forecast using the method described in section 5.2 produced superior agreement between predicted and observed parameters. This can be inferred from larger standard deviations in x and y components of wind in the last several hours of forecast calculation. Nudging of surface wind components that are not dynamically balanced with the numerical schemes of the model may be the reason for the results of the method in section 5.3. Temperature fields show little differences between the methods in sections 5.2 and 5.3 (nudging of individual surface wind data at initial time).

4. Surface data nudging every 3 h (section 5.4) produced the best agreements between calculation and observation. In this method, observed wind vector components were assimilated into model calculations by nudging every 3 h. Figure 35 shows smaller standard deviations at 3, 6, 9, and 12 h when the data were nudged during the previous 1 h. It should be noted that, although nudging of dynamically unbalanced wind vectors was done repeatedly, the numerical scheme of the model is stable enough to prevent numerical instability.

8. Summary

The forecasting skills of the BFM, developed at ARL for operational short-range (< 12 h) forecasting over battlescale areas (< 500 by 500 km), were evaluated. The BFM was applied to a model domain of 250 by 250 km covering WSMR, NM where observation data by SAMS and profilers are regularly available.

From the case study of wind field variation between 5 and 17 LST, 10 Mar 94, it became clear that wind fields interpolated from GSM data widely deviated from observed ones in the early morning hours because of the coarse grid spacing and the poor numerical schemes of boundary-layer physics of GSM. Thus, it was concluded that incorporation of observed surface wind data into the initial fields is important.

Three different BFM initialization methods were used to make 25 12-h forecasting cases. The initialization fields created by the three different methods were as follows:

1. GSM data interpolated fields of wind, temperature, and water vapor mixing ratio

2. Mean surface wind speed and direction based on observation in the boundary layer and GSM data interpolated upper air wind fields

3. Assimilation of observed surface wind vectors into the model by nudging during 1 h of the precomputation period

In all three methods, initial fields of temperature and water vapor were given by the interpolation of GSM output.

Comparison of forecast results using the method in section 5.1 (initialization using GSM) with space and time interpolation of GSM data clearly shows that the BFM produced substantially improved forecast fields over those using a simplistic interpolation of GSM data. Initialization using the methods in

sections 5.2 (initialization using GSM and mean surface wind direction and speed) and 5.3 (nudging of individual surface wind data at initialization) produced further improvement over the method in section 5.1, confirming that incorporation of observed data into initial fields is important.

In this study, all the cases were simulated in Feb and Mar 94, and forecast fields of moisture were not compared with observation because observed data were not considered reliable. In future studies supported by archived data, cases will be simulated during the summer.

Two statistical parameters, mean residual and standard deviation of mean residual for horizontal wind vector components and temperature, were calculated at every hour of forecast calculation by using 21 SAMS and 25 different cases.

References

1. Yamada, T., and S. Bunker, "A Numerical Study of Nocturnal Drainage Flows with Strong Wind and Temperature Gradients," *Journal of Applied Meteorology*, **28**, p 545-554, 1989.

2. Henmi, T., P. A. Tabor, and R. Flanigan, "Evaluation Study of Mesoscale Models Over Mountainous Regions," reprint of *4th Conference on Mountain Meteorology*, American Meteorological Society, Boston, MA, 1987.

3. Henmi, T., "Assimilation of Wind Field Over Complex Terrain," reprint volume of *5th Conference on Mountain Meteorology*, American Meteorological Society, Boston, MA, p 118-124, 1990.

4. Henmi, T., "Simulations of Meteorological Parameters Over a Complex Terrain," reprint of *6th Conference on Mountain Meteorology*, American Meteorological Society, Boston, MA, p 202-208, 1992.

5. Yamada, T., and S. Bunker, "Development of a Nested Grid, Second Moment Turbulence Closure Model and Application to the 1982 ASCOT Brush Creek Data Simulation," *Journal of Applied Meteorology*, **27**, p 562-578, 1988.

6. Mellor G. L., and T. Yamada, "Development of a Turbulence Closure Model for Geophysical Fluid Problems," *Review of Geophysics and Space Physics.*, **20**, p 851-875, 1982.

7. Dyer, A. J., and B. B. Hickes, "Flux-Gradient Relationships in the Constant Flux Layer," *Quarterly Journal of the Roy Meteorological Society*, **96**, p 715-721, 1970.

8. Yamada, T., "A Numerical Model Study of Turbulent Airflow in and Above a Forest Canopy," *Journal of Meteorological Society of Japan*, **60**, p 439-454, 1982.

9. Richtmyer, R. D., and K. W. Morton, *Difference Methods for Initial-Value Problems,* Second Ed., Interscience Publishers, J. Wiley and Sons, New York, p 405, 1967.

10. Yamada, T., and T. Henmi, "HOTMAC: Model Performance Evaluation by Issuing Project WIND Phase I and II Data in Mesoscale Modeling of the Atmosphere," *Meteorological Monographs*, American Meteorological Society, Boston, MA, **25**, No 47, p 123-135, 1993.

11. Yamada, T., "A Numerical Simulation of Nocturnal Drainage Flow," *Journal of Meteorological Society of Japan*, **59**, p 108-122, 1981.

12. Barnes, S. L., "A Technique for Maximizing Details in Numerical Weather Map Analysis," *Journal of Applied Meteorology*, **3**, p 396-409, 1964.

Acronyms and Abbreviations

APRF	Atmospheric Profiler Research Facility
ARL	Army Research Laboratory
BFM	Battlescale Forecast Model
GSM	Global Spectral Model
HOTMAC	Higher Order Turbulence Model for Atmospheric Circulation
LST	local standard time
SAMS	Surface Automated Meteorological System
3-D	three-dimensional
WSMR	White Sands Missile Range

Bibliography

Hoke, J. E., and R. A. Anthes, "The Initialization of Numerical Models by a Dynamic-Initialization Technique," *Monthly Weather Review*, **104**, p 1551-1556, 1976.

Yamada, T., "Simulations of Nocturnal Drainage Flows by a q^2l Turbulence Closure Model," *Journal of Atmospheric Science*, **40**, p 91-106, 1983.

Distribution

	Copies
ARMY CHEMICAL SCHOOL ATZN CM CC ATTN MR BARNES FT MCCLELLAN AL 36205-5020	1
NASA MARSHAL SPACE FLT CTR ATMOSPHERIC SCIENCES DIV E501 ATTN DR FICHTL HUNTSVILLE AL 35802	1
NASA SPACE FLT CTR ATMOSPHERIC SCIENCES DIV CODE ED 41 1 HUNTSVILLE AL 35812	1
ARMY STRAT DEFNS CMND CSSD SL L ATTN DR LILLY PO BOX 1500 HUNTSVILLE AL 35807-3801	1
ARMY MISSILE CMND AMSMI RD AC AD ATTN DR PETERSON REDSTONE ARSENAL AL 35898-5242	1
ARMY MISSILE CMND AMSMI RD AS SS ATTN MR H F ANDERSON REDSTONE ARSENAL AL 35898-5253	1
ARMY MISSILE CMND AMSMI RD AS SS ATTN MR B WILLIAMS REDSTONE ARSENAL AL 35898-5253	1

ARMY MISSILE CMND 1
AMSMI RD DE SE
ATTN MR GORDON LILL JR
REDSTONE ARSENAL
AL 35898-5245

ARMY MISSILE CMND 1
REDSTONE SCI INFO CTR
AMSMI RD CS R DOC
REDSTONE ARSENAL
AL 35898-5241

ARMY MISSILE CMND 1
AMSMI
REDSTONE ARSENAL
AL 35898-5253

ARMY INTEL CTR 1
AND FT HUACHUCA
ATSI CDC C
FT HUACHUCA AZ 85613-7000

NORTHROP CORPORATION 1
ELECTR SYST DIV
ATTN MRS T BROHAUGH
2301 W 120TH ST BOX 5032
HAWTHORNE CA 90251-5032

NAVAL WEAPONS CTR 1
CODE 3331
ATTN DR SHLANTA
CHINA LAKE CA 93555

PACIFIC MISSILE TEST CTR 1
GEOPHYSICS DIV
ATTN CODE 3250
POINT MUGU CA 93042-5000

LOCKHEED MIS & SPACE CO 1
ATTN KENNETH R HARDY
ORG 91 01 B 255
3251 HANOVER STREET
PALO ALTO CA 94304-1191

NAVAL OCEAN SYST CTR 1
CODE 54
ATTN DR RICHTER
SAN DIEGO CA 92152-5000

METEOROLOGIST IN CHARGE 1
KWAJALEIN MISSILE RANGE
PO BOX 67
APO SAN FRANCISCO
CA 96555

DEPT OF COMMERCE CTR 1
MOUNTAIN ADMINISTRATION
SPPRT CTR LIBRARY R 51
325 S BROADWAY
BOULDER CO 80303

DR HANS J LIEBE 1
NTIA ITS S 3
325 S BROADWAY
BOULDER CO 80303

NCAR LIBRARY SERIALS 1
NATL CTR FOR ATMOS RSCH
PO BOX 3000
BOULDER CO 80307-3000

DEPT OF COMMERCE CTR 1
325 S BROADWAY
BOULDER CO 80303

DAMI POI 1
WASH DC 20310-1067

MIL ASST FOR ENV SCI OFC 1
OF THE UNDERSEC OF DEFNS
FOR RSCH & ENGR R&AT E LS
PENTAGON ROOM 3D129
WASH DC 20301-3080

DEAN RMD 1
ATTN DR GOMEZ
WASH DC 20314

SPACE NAVAL WARFARE
SYST CMND
PMW 145 1G
WASH DC 20362-5100 1

ARMY INFANTRY
ATSH CD CS OR
ATTN DR E DUTOIT
FT BENNING GA 30905-5090 1

AIR WEATHER SERVICE
TECH LIBRARY FL4414 3
SCOTT AFB IL 62225-5458 1

USAFETAC DNE
ATTN MR GLAUBER
SCOTT AFB IL 62225-5008 1

HQ AWS DOO 1
SCOTT AFB IL 62225-5008 1

ARMY SPACE INSTITUTE
ATTN ATZI SI 3
FT LEAVENWORTH
KS 66027-5300 1

PHILLIPS LABORATORY
PL LYP
ATTN MR CHISHOLM
HANSCOM AFB MA 01731-5000 1

ATMOSPHERIC SCI DIV
GEOPHYSICS DIRCTRT
PHILLIPS LABORATORY
HANSCOM AFB MA 01731-5000 1

PHILLIPS LABORATORY
PL LYP 3
HANSCOM AFB MA 01731-5000 1

RAYTHEON COMPANY
ATTN DR SONNENSCHEIN
528 BOSTON POST ROAD
SUDBURY MA 01776
MAIL STOP 1K9 1

ARMY MATERIEL SYST 1
ANALYSIS ACTIVITY
AMXSY
ATTN MP H COHEN
APG MD 21005-5071

ARMY MATERIEL SYST 1
ANALYSIS ACTIVITY
AMXSY AT
ATTN MR CAMPBELL
APG MD 21005-5071

ARMY MATERIEL SYST 1
ANALYSIS ACTIVITY
AMXSY CR
ATTN MR MARCHET
APG MD 21005-5071

ARL CHEMICAL BIOLOGY 1
NUC EFFECTS DIV
AMSRL SL CO
APG MD 21010-5423

ARMY MATERIEL SYST 1
ANALYSIS ACTIVITY
AMXSY
APG MD 21005-5071

NAVAL RESEARCH LABORATORY 1
CODE 4110
ATTN MR RUHNKE
WASH DC 20375-5000

ARMY MATERIEL SYST 1
ANALYSIS ACTIVITY
AMXSY CS
ATTN MR BRADLEY
APG MD 21005-5071

ARMY RESEARCH LABORATORY 1
AMSRL D
2800 POWDER MILL ROAD
ADELPHI MD 20783-1145

ARMY RESEARCH LABORATORY 1
AMSRL OP SD TP
TECHNICAL PUBLISHING
2800 POWDER MILL ROAD
ADELPHI MD 20783-1145

ARMY RESEARCH LABORATORY 1
AMSRL OP CI SD TL
2800 POWDER MILL ROAD
ADELPHI MD 20783-1145

ARMY RESEARCH LABORATORY 1
AMSRL SS SH
ATTN DR SZTANKAY
2800 POWDER MILL ROAD
ADELPHI MD 20783-1145

ARMY RESEARCH LABORATORY 1
AMSRL
2800 POWDER MILL ROAD
ADELPHI MD 20783-1145

NATIONAL SECURITY AGCY W21 1
ATTN DR LONGBOTHUM
9800 SAVAGE ROAD
FT GEORGE G MEADE
MD 20755-6000

ARMY AVIATION CTR 1
ATZQ D MA
ATTN MR HEATH
FT RUCKER AL 36362

OIC NAVSWC 1
TECH LIBRARY CODE E 232
SILVER SPRINGS
MD 20903-5000

ARMY RSRC OFC 1
ATTN DRXRO GS
PO BOX 12211
RTP NC 27009

DR JERRY DAVIS 1
NCSU
PO BOX 8208
RALEIGH NC 27650-8208

ARMY CCREL
CECRL GP
ATTN DR DETSCH
HANOVER NH 03755-1290 1

ARMY ARDEC
SMCAR IMI I BLDG 59
DOVER NJ 07806-5000 1

ARMY SATELLITE COMM AGCY
DRCPM SC 3
FT MONMOUTH NJ 07703-5303 1

ARMY COMMUNICATIONS
ELECTR CTR FOR EW RSTA
AMSEL EW D
FT MONMOUTH NJ 07703-5303 1

ARMY COMMUNICATIONS
ELECTR CTR FOR EW RSTA
AMSEL EW MD
FT MONMOUTH NJ 07703-5303 1

ARMY DUGWAY PROVING GRD
STEDP MT DA L 3
DUGWAY UT 84022-5000 1

ARMY DUGWAY PROVING GRD
STEDP MT M
ATTN MR BOWERS
DUGWAY UT 84022-5000 1

DEPT OF THE AIR FORCE
OL A 2D WEATHER SQUAD MAC
HOLLOMAN AFB
NM 88330-5000 1

PL WE
KIRTLAND AFB NM
87118-6008 1

USAF ROME LAB TECH
CORRIDOR W STE 262 RL SUL
26 ELECTR PKWY BLD 106
GRIFFISS AFB
NY 13441-4514 1

AFMC DOW 1
WRIGHT PATTERSON AFB
OH 0334-5000

ARMY FIELD ARTLLRY SCHOOL 1
ATSF TSM TA
FT SILL OK 73503-5600

NAVAL AIR DEV CTR 1
CODE 5012
ATTN AL SALIK
WARMINISTER PA 18974

ARMY FOREGN SCI TECH CTR 1
CM
220 7TH STREET NE
CHARLOTTESVILLE
VA 22901-5396

NAVAL SURFACE WEAPONS CTR 1
CODE G63
DAHLGREN VA 22448-5000

ARMY OEC 1
CSTE EFS
PARK CENTER IV
4501 FORD AVE
ALEXANDRIA VA 22302-1458

ARMY CORPS OF ENGRS 1
ENGR TOPOGRAPHICS LAB
ETL GS LB
FT BELVOIR VA 22060

TAC DOWP 1
LANGLEY AFB
VA 23665-5524

ARMY TOPO ENGR CTR 1
CETEC ZC 1
FT BELVOIR VA 22060-5546

LOGISTICS CTR 1
ATCL CE
FT LEE VA 23801-6000

SCI AND TECHNOLOGY 1
101 RESEARCH DRIVE
HAMPTON VA 23666-1340

ARMY NUCLEAR CML AGCY 1
MONA ZB BLDG 2073
SPRINGFIELD VA 22150-3198

ARMY FIELD ARTLLRY SCHOOL 1
ATSF F FD
FT SILL OK 73503-5600

USATRADOC 1
ATCD FA
FT MONROE VA 23651-5170

ARMY TRADOC ANALYSIS CTR 1
ATRC WSS R
WSMR NM 88002-5502

ARMY RESEARCH LABORATORY 1
AMSRL BE M
BATTLEFIELD ENVIR DIR
WSMR NM 88002-5501

ARMY RESEARCH LABORATORY 1
AMSRL BE A
BATTLEFIELD ENVIR DIR
WSMR NM 88002-5501

ARMY RESEARCH LABORATORY 1
AMSRL BE W
BATTLEFIELD ENVIR DIR
WSMR NM 88002-5501

ARMY RESEARCH LABORATORY 1
AMSRL BE
ATTN MR VEAZEY
BATTLEFIELD ENVIR DIR
WSMR NM 88002-5501

DEFNS TECH INFO CTR 1
CENTER DTIC BLS
BLDG 5 CAMERON STATION
ALEXANDRIA
VA 22304-6145

ARMY MISSILE CMND AMSMI REDSTONE ARSENAL AL 35898-5243	1
ARMY DUGWAY PROVING GRD STEDP 3 DUGWAY UT 84022-5000	1
USATRADOC ATCD FA FT MONROE VA 23651-5170	1
ARMY FIELD ARTLRY SCHOOL ATSF FT SILL OK 73503-5600	1
WSMR TECH LIBRARY BR STEWS IM IT WSMR NM 88001	1
Record Copy	10
TOTAL	96